

Equilibrium solvation in quadrupolar solvents

Anatoli A. Milischuk and Dmitry V. Matyushov*

Department of Chemistry and Biochemistry, Arizona State University, PO Box 871604, Tempe, AZ 85287-1604

(Dated: October 17, 2018)

We present a microscopic theory of equilibrium solvation in solvents with zero dipole moment and non-zero quadrupole moment (quadrupolar solvents). The theory is formulated in terms of autocorrelation functions of the quadrupolar polarization (structure factors). It can be therefore applied to an arbitrary dense quadrupolar solvent for which the structure factors are defined. We formulate a simple analytical perturbation treatment for the structure factors. The solute is described by coordinates, radii, and partial charges of constituent atoms. The theory is tested on Monte Carlo simulations of solvation in model quadrupolar solvents. It is also applied to the calculation of the activation barrier of electron transfer reactions in a cleft-shaped donor-acceptor complex dissolved in benzene with the structure factors of quadrupolar polarization obtained from Molecular Dynamics simulations.

I. INTRODUCTION

The understanding of kinetics of chemical reactions in non-polar or, more generally, non-dipolar solvents poses the necessity to describe thermodynamic^{1,2,3,4,5,6} and dynamic^{7,8,9,10,11} aspects of non-polar solvation.¹² The overall solvation free energy in a non-dipolar solvent (zero permanent dipole) can be approximately separated into the contribution from the solute repulsive core (cavitation energy), the attractive dispersion solvation, and electrostatic contributions from induced dipoles and permanent multipoles starting from the quadrupole moment. The cavitation energy is often described by models considering the free energy necessary to insert the solute hard repulsive core into the solvent.^{13,14,15,16,17} The dispersion energy is a very significant part of solvation energetics even in polar solvents.¹⁸ It is normally modeled by site-site Lennard-Jones (LJ) interaction potentials, although LJ parameterization is often obscure for molecular excited states.

The positive cavitation free energy and negative contributions from dispersion and electrostatic interactions cancel each other in the overall solvation free energy which often constitutes only a small portion of each component. The cavitation and dispersion energies, however, cancel almost identically when the absorption and emission solvatochromic shifts are subtracted to form the optical Stokes shift or when the solvent reorganization energy of electron transfer (ET) is calculated.^{1,18} The remaining contribution from dispersion interactions, normally associated with mechanical solvation,^{19,20} does not typically exceed $100-200\text{ cm}^{-1}$, which is small compared to usual values of the Stokes shift arising from dipolar and quadrupolar solvation.² The electrostatic component of solvation free energy in non-dipolar solvents arising from (partial) solute charges interacting with solvent quadrupoles is the focus of the present equilibrium solvation theory.

The electrostatic component of non-dipolar solvation, in particular quadrupolar solvation, has received little attention^{2,3,4,6,21,22,23,24} compared to the very extensive literature on solvation in dipolar solvents.^{6,25,26} In contrast to dipolar solvation, where dielectric measurements provide the basis for modeling thermodynamics and dynamics of solvation,^{25,27,28,29,30,31} there is no obvious method to extract the dynamic and thermodynamic response functions in non-dipolar solvents from existing data. This paper aims at bridging this gap by formulating a microscopic solvation theory in terms of correlation functions of quadrupolar polarization of the pure solvent. In this paper, we limit the solvent correlation functions to the spatial domain thus gaining access to the equilibrium solvation thermodynamics. Once dynamic correlation functions become available, the theory can be extended to solvation dynamics.

The experimental evidence on electrostatic quadrupolar solvation comes from the realm of steady-state^{2,32,33} and time-resolved^{2,4} optical spectroscopy, resonance Raman spectroscopy,^{34,35} and from the kinetics of electron transfer (ET) reactions.³⁶ Spectroscopic chromophores and ET solutes are normally large molecules with complex molecular shape. Because of the relatively short range of interaction of molecular solvent quadrupoles with solute partial charges, it might be critical to include the correct molecular shape of the solute into the formalism. We therefore sacrifice some accuracy of the modeling compared to potentially more accurate perturbation models for spherical solutes⁵ in order to introduce the molecular shape of the solute with atomic resolution combined with molecular charge distribution specified by atomic partial charges. It appears that this is the first theory of quadrupolar solvation approaching this level of detail in describing the solute.

The paper starts with the formulation of the problem (Sec. II) followed by the formal theory of solvation thermodynamics (Sec. III). The perturbation theory is given in terms of structure factors of fluctuating quadrupolar polarization in the pure solvent discussed in Sec. IV. The theory is tested on computer simulations of model ionic and dipolar solutes in Sec. V and is compared to exper-

*E-mail:dmitrym@asu.edu.

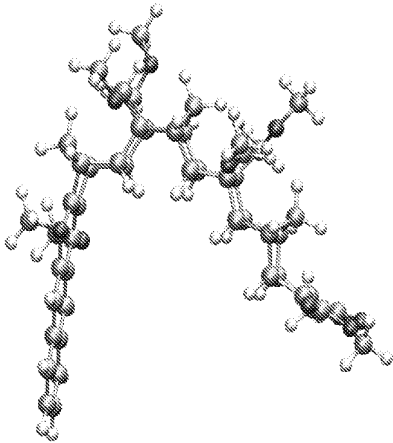


FIG. 1: Charge transfer complex combining dymethoxyanthracene unit for the donor (D) and a cyclobutene dicarboxylate derivative for an acceptor (A) connected by a bridge (B).³⁶ The present theory is applied to the activated kinetics of charge separation, $DB^*A \rightarrow D^+BA^-$.

imental ET kinetics in Sec. VI. ET kinetics in a donor-bridge-acceptor cleft molecule referred to as complex **1** (Fig. 1) has been extensively studied by Waldeck and Zimmt.³⁶ The present theory is applied to the kinetic data in benzene used as a solvent. As a consistency test, the parameters used for ET rates in benzene are applied to ET in acetonitrile with the previously developed theory of polar solvation.^{37,38} The overall good agreement between theory and experiment is reported.

II. CONCEPTUAL FRAMEWORK

Solvation in polar solvents is defined by the coupling of the field $\mathbf{E}_0(\mathbf{r})$ of the solute to the dipolar polarization of the solvent $\mathbf{P}(\mathbf{r})$. The interaction potential of the solute (subscript “0”) with the solvent (subscript “s”) is then a composite effect of this coupling integrated over the space occupied by the solvent Ω

$$v_{0s}[\mathbf{P}] = - \int_{\Omega} \mathbf{P}(\mathbf{r}) \cdot \mathbf{E}_0(\mathbf{r}) d\mathbf{r}. \quad (1)$$

Here, the dipolar polarization is defined by the density of permanent dipoles \mathbf{m}_j in the liquid

$$\mathbf{P}(\mathbf{r}) = \sum_j \mathbf{m}_j \delta(\mathbf{r} - \mathbf{r}_j), \quad (2)$$

where the sum runs over N molecules of the solvent with center-of-mass coordinates \mathbf{r}_j . In the linear response approximation (LRA), the above interaction energy is supplemented by the Gaussian Hamiltonian³⁹

$$H_P[\mathbf{P}] = \frac{1}{2} \int \mathbf{P}(\mathbf{r}) \cdot \chi_P(\mathbf{r}, \mathbf{r}')^{-1} \cdot \mathbf{P}(\mathbf{r}') d\mathbf{r} d\mathbf{r}', \quad (3)$$

where the polarization response function $\chi_P(\mathbf{r}, \mathbf{r}')$ generally depends on the shape of the field source. For certain geometries, e.g. for a parallel plate capacitor, the dependence on geometry can be eliminated. The polarization induced in the solvent by the external electric field $\mathbf{E}_0(\mathbf{r})$ is then obtained by minimizing the functional $v_{0s}[\mathbf{P}] + H_P[\mathbf{P}]$ in $\mathbf{P}(\mathbf{r})$ to yield

$$\mathbf{P}(\mathbf{r}) = \int_{\Omega} \chi_P(\mathbf{r}, \mathbf{r}') \cdot \mathbf{E}_0(\mathbf{r}') d\mathbf{r}'. \quad (4)$$

Molecular quadrupoles couple to an inhomogeneous electric field with the gradient $\nabla \mathbf{E}_0(\mathbf{r})$

$$v_{0s}[\mathbf{Q}] = -(1/3) \int_{\Omega} \mathbf{Q}(\mathbf{r}) : \nabla \mathbf{E}_0(\mathbf{r}) d\mathbf{r}, \quad (5)$$

where the quadrupolar polarization is

$$\mathbf{Q}(\mathbf{r}) = \sum_j \mathbf{Q}_j \delta(\mathbf{r} - \mathbf{r}_j) \quad (6)$$

and \mathbf{Q}_j is the molecular quadrupole tensor. Similarly to Eq. (3), the Hamiltonian of the quadrupolar polarization in the pure solvent is given in the Gaussian form

$$H_Q[\mathbf{Q}] = \frac{1}{2} \int_{\Omega} \mathbf{Q}(\mathbf{r}) : \chi_Q(\mathbf{r}, \mathbf{r}')^{-1} : \mathbf{Q}(\mathbf{r}') d\mathbf{r} d\mathbf{r}'. \quad (7)$$

The minimization of $v_{0s}[\mathbf{Q}] + H_Q[\mathbf{Q}]$ in terms of $\mathbf{Q}(\mathbf{r})$ then leads to

$$\mathbf{Q}(\mathbf{r}) = \frac{1}{3} \int_{\Omega} \chi_Q(\mathbf{r}, \mathbf{r}') : \nabla \mathbf{E}_0(\mathbf{r}') d\mathbf{r}'. \quad (8)$$

The definition of response functions $\chi_P(\mathbf{r}, \mathbf{r}')$ and $\chi_Q(\mathbf{r}, \mathbf{r}')$ incorporates the non-local solvent response affected by finite-range microscopic correlations of molecular dipoles and quadrupoles. These correlations are neglected in the continuum approximation

$$\chi_{P,Q}(\mathbf{r}, \mathbf{r}') = \delta(\mathbf{r} - \mathbf{r}') \chi_{P,Q}(\mathbf{r}). \quad (9)$$

The continuum approximation, used in dielectric continuum models of dipolar⁴⁰ and non-dipolar^{22,23} solvation, significantly simplifies the calculation of the polar response function. In particular, the dipolar response function can be related to the macroscopic dielectric properties of the solvent through the macroscopic material Maxwell’s equations.

The Maxwell’s equation for the overall electric field in the dielectric \mathbf{E} reads⁴¹

$$\nabla \cdot (\mathbf{E} + 4\pi \mathbf{P}) = 4\pi \rho + 4\pi \nabla \cdot (\nabla \cdot \mathbf{Q}). \quad (10)$$

The material equations are closed by defining the dielectric displacement $\mathbf{D} = \mathbf{E} + 4\pi \mathbf{P}$ which is connected to the density of external charges ρ by the relation neglecting the quadrupolar density in the right hand part of Eq. (10)

$$\nabla \cdot \mathbf{D} = 4\pi \rho. \quad (11)$$

The dielectric displacement is in turn related to the overall electric field through the static dielectric constant ϵ_s , $\mathbf{D} = \epsilon_s \mathbf{E}$. In the case of a parallel plate capacitor, $\mathbf{D} = \mathbf{E}_0$ and one gets

$$\chi_P = (\epsilon_s - 1)/4\pi\epsilon_s. \quad (12)$$

More complex geometries of the field source require solving the Poisson equation with the boundary conditions defined by the dielectric constant and the shape of the dielectric. This procedure establishes the widely used dielectric continuum approximation for the dipolar response.

Many of the advantages of the dielectric continuum approximation disappear when applied to quadrupolar (non-dipolar) solvation. The main problem is that the continuum quadrupolar susceptibility χ_Q does not come to the material Maxwell's equations and is, therefore, not directly related to any well-established experimental protocol. Measuring quadrupolar susceptibility is still a non-trivial experimental problem.⁴² In practical continuum calculations of the quadrupolar response, the quadrupolar susceptibility is obtained by fitting the calculated response to solvation free energies from spectroscopy.²³ One would alternatively want to have the quadrupolar susceptibility from properties of a pure quadrupolar solvent unaffected by all the complexities of treating spectral band-shapes of complex molecular solutes. In addition, one needs to know the limits of applicability of the continuum approximation [Eq. (9)] to relatively short-ranged quadrupolar interactions. The high directionality of quadrupolar forces make them unlike candidates for mean-field theories which are successfully applied to short-range but more isotropic dispersion forces.^{43,44} All these considerations call for the necessity of microscopic theories of quadrupolar solvation. Once such a theory is formulated, approximate solutions, e.g. the continuum limit, can be obtained in a more controlled fashion. The formulation of such a theory is a goal of this paper.

In order to develop a theory applicable to solutes of complex shape, we use a particular expression of the LRA to obtain the chemical potential of solvation μ_{0s} . Within the LRA, μ_{0s} can be calculated as the second cumulant of the solute-solvent interaction potential⁴⁵

$$-\mu_{0s} = (\beta/2) \langle \delta v_{0s}^2 \rangle_0, \quad (13)$$

where $\beta = 1/k_B T$, k_B is Boltzmann's constant and T is the temperature. The statistical average $\langle \dots \rangle_0$ is over the solvent configurations around a fictitious solute with the solute-solvent interaction energy v_{0s} eliminated from the total interaction energy. The calculation of the average $\langle \dots \rangle_0$ over the solvent configurations in the presence of the repulsive core of the solute is a major challenge for the theory development. The solute expels the solvent from its volume and may significantly modify the statistics of solvent fluctuations either by altering the local density profile of the solvent or/and the statistics of orientational fluctuations of the solvent molecules.³⁹

The expulsion effect propagates through the entire solvent changing substantially the solvent response function in strongly dipolar liquids.^{46,47} This strong effect of the solute on solvent statistics arises from the long range character of dipole-dipole interactions accounted for in dielectric models through the boundary conditions in the Poisson equation.

The quadrupole-quadrupole interaction is much more short-range compared to the dipole-dipole interaction ($\propto 1/r^5$ vs $\propto 1/r^3$). One may expect that statistics of orientational quadrupolar fluctuations is not significantly altered by the solute which only expels the solvent quadrupoles from its volume. In this approximation, one can switch from the statistical average $\langle \dots \rangle_0$ to the average $\langle \dots \rangle$ over the statistical configurations of the pure solvent by replacing $v_{0s}(\mathbf{r})$ in Eq. (13) with $v_{0s}(\mathbf{r})\theta(\mathbf{r})$, where $\theta(\mathbf{r})$ is a step function equal to zero inside the solute and equal to one everywhere else.

We will denote the component of the solvation chemical potential arising from fluctuations of quadrupolar polarization in homogeneous solvent as μ_{0s}^Q (superscript "Q" stands for quadrupolar polarization). This component is expected to be the major contribution to the quadrupolar solvation chemical potential. However, in addition to expelling quadrupolar polarization from its volume, insertion of a solute into a liquid creates a nonuniform density profile represented by the solute-solvent pair correlation function $h_{0s}(\mathbf{r})$. This correlation function, highly specific to the solute shape and the thermodynamic state of the solvent, can be reliably calculated only for simple solute geometries. The component of μ_{0s} associated with $h_{0s}(\mathbf{r})$ will be denoted as μ_{0s}^D (superscript "D" refers to the local density profile). The overall chemical potential of solvation is a sum of the long-range component due to quadrupolar orientational fluctuations ("Q" component) and the short-range component due to the local density profile ("D" component):

$$\mu_{0s} = \mu_{0s}^Q + \mu_{0s}^D. \quad (14)$$

III. PERTURBATION THEORY OF SOLVATION

The solute-solvent interaction potential in Eq. (5) can be written either in Cartesian or spherical coordinates. We will use Greek indexes for the Cartesian projections and Latin indexes for the spherical projections.⁴⁸ In the Cartesian projections, the solute electric field gradient and the quadrupolar polarization are given as follows

$$\phi_{\alpha\beta}(\mathbf{r}) = -\nabla_\alpha E_\beta = -\nabla_\alpha \nabla_\beta \sum_{a=1}^M \frac{q_0^a}{|\mathbf{r} - \mathbf{r}_0^a|} \quad (15)$$

and

$$Q_{\alpha\beta}(\mathbf{r}) = \sum_j Q_{\alpha\beta,j} \delta(\mathbf{r} - \mathbf{r}_j). \quad (16)$$

The sum (index a) in Eq. (15) runs over the M solute (subscript "0") atoms with coordinates \mathbf{r}_0^a and partial

charges q_j^a . In Eq. (16), the summation is over N solvent molecules with centers of mass at \mathbf{r}_j relative to which the quadrupole tensor $Q_{\alpha\beta,j}$ is defined as:

$$Q_{\alpha\beta,j} = (1/2) \sum_{a=1}^K q_j^a (r_j^a)^2 (3\hat{r}_{\alpha,j}^a \hat{r}_{\beta,j}^a - \delta_{\alpha\beta}). \quad (17)$$

Here, the sum (index a) runs over the K atoms of the solvent molecule with coordinates $\mathbf{r}_j + \hat{\mathbf{r}}_j^a r_j^a$ ($\hat{\mathbf{r}}_j^a = \mathbf{r}_j^a / r_j^a$) and partial charges q_j^a .

In the spherical projections one gets

$$v_{0s} = \sum_{m,j} \int \phi_{2m}(\mathbf{r}) Q_{2m,j}^* d\mathbf{r}, \quad (18)$$

where the spherical projections of the quadrupolar polarization

$$Q_{2m}(\mathbf{r}) = \sum_j Q_{2m,j} \delta(\mathbf{r} - \mathbf{r}_j) \quad (19)$$

are given in terms of the spherical quadrupolar tensor

$$Q_{2m,j} = \sum_{a=1}^K q_j^a (r_j^a)^2 Y_{2m}(\hat{\mathbf{r}}_j^a). \quad (20)$$

In Eq. (20), $Y_{2m}(\hat{\mathbf{r}})$ is the spherical harmonic of the second order, $-2 \leq m \leq 2$. The distribution of molecular charge is illustrated in Fig. 2 on the example of the benzene molecule the first non-zero multipole of which is quadrupole.

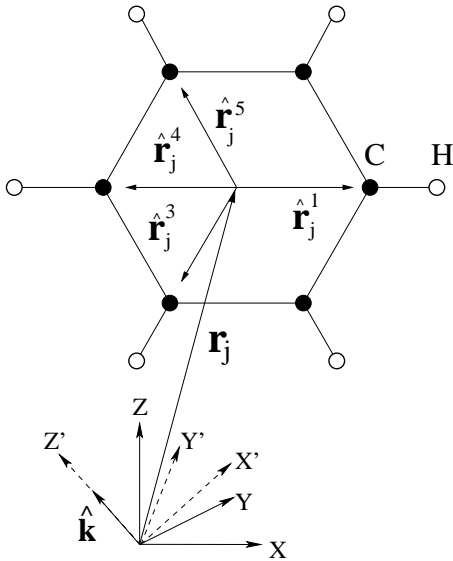


FIG. 2: The schematic representation of the benzene molecule: \mathbf{r}_j is the coordinate of the center of mass, $\hat{\mathbf{r}}_j^a$ are unit vectors in the direction of partial charges q_j^a . XYZ is the laboratory coordinate frame, the Z' axis of the laboratory system $X'Y'Z'$ is along the unit wavevector $\hat{\mathbf{k}} = \mathbf{k}/k$.

Substituting v_{0s} from Eq. (18) into Eq. (13) and switching to the \mathbf{k} -space we obtain

$$\mu_{0s}^Q = -\frac{\beta\rho Q^2}{8\pi} \sum_{m,n} \int \frac{d\mathbf{k}}{(2\pi)^3} \tilde{\phi}_{2m}(-\mathbf{k}) \tilde{\phi}_{2n}^*(\mathbf{k}) S_{mn}(k). \quad (21)$$

Here, $\tilde{\phi}_{2m}$ is the Fourier transform of ϕ_{2m} , $\tilde{\phi}_{2n}^*$ is the Fourier transform of ϕ_{2n}^* , and

$$Q^2 = (2/3)\mathbf{Q} : \mathbf{Q} \quad (22)$$

is the rotational-invariant ‘‘effective axial quadrupole moment’’.⁴⁸ The correlation function $S_{mn}(k)$ in Eq. (21) does not depend on the orientation of the wavevector because of the rotational isotropy of the solvent:

$$S_{mn}(k) = \frac{4\pi}{NQ^2} \left\langle \sum_{i,j} Q_{2m,i}^* Q_{2n,j} e^{i\mathbf{k}\cdot\mathbf{r}_{ij}} \right\rangle. \quad (23)$$

Since μ_{0s}^Q is invariant with respect to rotations of the coordinate system we first consider $\tilde{\phi}_{2m}$ and S_{mn} in the coordinate system $X'Y'Z'$ in which the wavevector \mathbf{k} is directed along the Z' -axis (Fig. 2). The functions of \mathbf{k} in this coordinate system will be specified with the prime. The wavevector \mathbf{k} introduces axial symmetry in the otherwise isotropic liquid of solvent molecules. The operation of statistical average must therefore commute with the operation of rotation about the wavevector \mathbf{k}

$$\exp(-i\hat{l}_z\gamma) S'_{mn} \exp(i\hat{l}_z\gamma) = \exp(i(m-n)\gamma) S'_{mn}, \quad (24)$$

where \hat{l}_z is the operator of rotation through the angle γ . The condition of invariance requires $m = n$ leading to a simplified form of Eq. (21)

$$\mu_{0s}^Q = -\frac{\beta\rho Q^2}{8\pi} \sum_{m=0}^2 \int \frac{d\mathbf{k}}{(2\pi)^3} \tilde{\phi}'^m(\mathbf{k}) S'^m(k). \quad (25)$$

In Eq. (25) we represent $\tilde{\phi}'^m(\mathbf{k})$ as

$$\begin{aligned} \tilde{\phi}'^0(\mathbf{k}) &= \tilde{\phi}'_0(\mathbf{k}), \\ \tilde{\phi}'^1(\mathbf{k}) &= \frac{1}{2}(\tilde{\phi}'_1(\mathbf{k}) + \tilde{\phi}'_{\underline{1}}(\mathbf{k})), \\ \tilde{\phi}'^2(\mathbf{k}) &= \frac{1}{2}(\tilde{\phi}'_2(\mathbf{k}) + \tilde{\phi}'_{\underline{2}}(\mathbf{k})), \end{aligned} \quad (26)$$

where ($\underline{m} = -m$) and

$$\tilde{\phi}'_m(\mathbf{k}) = \frac{\tilde{\phi}_{2m}(-\mathbf{k}) \tilde{\phi}_{2m}^*(\mathbf{k})}{4\pi}. \quad (27)$$

Quadrupolar structure factors $S'^m(k)$ in Eq. (25) are defined as

$$\begin{aligned} S'^0(k) &= S'_0(k), \\ S'^1(k) &= S'_1(k) + S'_{\underline{1}}(k), \\ S'^2(k) &= S'_2(k) + S'_{\underline{2}}(k), \end{aligned} \quad (28)$$

where

$$S'_m(k) = \frac{4\pi}{NQ^2} \left\langle \sum_{i,j} (Q')_{2m,i}^* (Q')_{2m,j} e^{i\mathbf{k}\cdot\mathbf{r}_{ij}} \right\rangle. \quad (29)$$

Three quadrupolar structure factors $S^m(k)$, grouped according to rotational symmetry, form a minimal set of correlation functions describing collective fluctuations of the quadrupolar polarization. Note that two structure factors representing uncoupled longitudinal and transverse dipolar polarization are sufficient to describe orientational fluctuations in dipolar solvents.^{37,49} Numerical calculations are more convenient to carry out in Cartesian coordinates in which the chemical potential of solvation and the structure factors can be re-written as (Appendix A)

$$\mu_{0s}^Q = -\frac{\beta\rho Q^2}{2} \sum_{m=0}^2 \int \frac{d\mathbf{k}}{(2\pi)^3} \tilde{\phi}^m(\mathbf{k}) S^m(k). \quad (30)$$

Here, $\tilde{\phi}^m(\mathbf{k})$ the structure factors $S^m(k)$ are expressed in the form of rotation-invariant tensor contractions in Eq. (A6) and Eq. (A5) respectively.

The density component of the solvation chemical potential in Eq. (14) is calculated by perturbation expansion with the solute-solvent pair correlation function $h_{0s}^{(0)}(\mathbf{r})$ corresponding to the distribution of the solvent around the repulsive core of the solute unaffected by the solute-solvent interaction potential v_{0s} (reference system)⁵⁰

$$\mu_{0s}^D = -(\beta\rho/18) \int d\mathbf{r} h_{0s}^{(0)}(\mathbf{r}) (\phi(\mathbf{r}) : \mathbf{Q})^2. \quad (31)$$

IV. QUADRUPOLEAR STRUCTURE FACTORS

The k -dependent quadrupolar structure factors determine the microscopic spatial correlations of the quadrupolar polarization in the homogeneous solvent. Dipolar structure factors of model dipolar fluids^{37,51,52} and fluids defined by site-site interaction potentials^{6,53,54,55,56,57,58} have been rather extensively studied in the literature. On the other hand, calculations of the quadrupolar structure factors have never been attempted before. Note that both dipolar and quadrupolar structure factors are unavailable from experiment, and liquid state theories and computer experiment are the only source of this information. We present here the results of Monte Carlo (MC) simulations of structure factors of quadrupolar hard-sphere fluids (simulation details are given in Appendix B). This is followed by an approximate analytical theory aiming at a fast algorithm applicable to calculations of solvation thermodynamics. In addition, the quadrupolar structure factors for benzene used in modeling ET reactions in Sec. VII were obtained from Molecular Dynamics (MD) simulations of the 12-site nonpolarizable, rigid force field (Fig. 2) with the

quadrupole moment $Q = 8.63 \text{ D}\times\text{\AA}$ (simulation details are given in Appendix C).

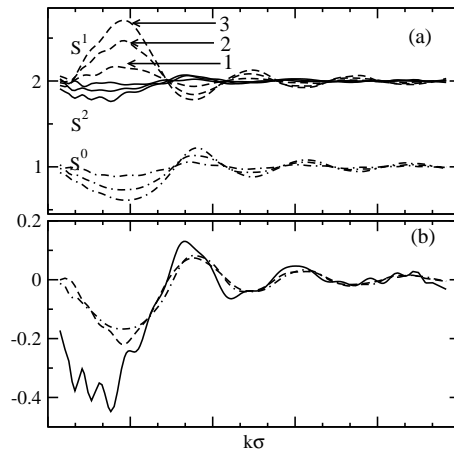


FIG. 3: (a) Quadrupolar structure factors for fluids of hard spheres with embedded point axial quadrupoles: $\rho^* = 0.8$, $(Q^*)^2 = 0.1$ (1), 0.3 (2), and 0.5 (3). (b) $(S^0(k) - 1)5/8$ (dash-dotted line), $-(S^1(k) - 2)15/32$ (dashed line), and $(S^2 - 2)15/8$ (solid line) with $S^m(k)$ from MC simulations at $(Q^*)^2 = 0.3$.

The quadrupolar structure factors $S^m(k)$ of a fluid of linear quadrupoles can be represented in terms of scalar products of unit vectors $\hat{\mathbf{e}}_j$ along the principle axes of the molecule and the direction of the wavevector $\hat{\mathbf{k}} = \mathbf{k}/k$. Adopting the notation of Ref. 59, $T_{ij} = (\hat{\mathbf{e}}_i \cdot \hat{\mathbf{e}}_j) - (\hat{\mathbf{e}}_i \cdot \hat{\mathbf{k}})(\hat{\mathbf{e}}_j \cdot \hat{\mathbf{k}})$ and $T_j = (\hat{\mathbf{e}}_j \cdot \hat{\mathbf{k}})$, one gets

$$\begin{aligned} S^0(k) &= \frac{5}{4N} \left\langle \sum_{ij} (3T_i^2 - 1)(3T_j^2 - 1) e^{i\mathbf{k}\cdot\mathbf{r}_{ij}} \right\rangle, \\ S^1(k) &= \frac{15}{N} \left\langle \sum_{ij} T_{ij} T_i T_j e^{i\mathbf{k}\cdot\mathbf{r}_{ij}} \right\rangle, \\ S^2(k) &= \frac{15}{4N} \left\langle \sum_{ij} [2T_{ij}^2 - (1 - T_i^2)(1 - T_j^2)] e^{i\mathbf{k}\cdot\mathbf{r}_{ij}} \right\rangle. \end{aligned} \quad (32)$$

The axial-quadrupole structure factors $S^m(k)$ can also be expressed in terms of projections of the solvent-solvent pair correlation function on rotational invariants as follows

$$\begin{aligned} S^0(k) &= 1 - \frac{2}{5}\rho \left(\tilde{h}^{220}(k) - \tilde{h}^{222}(k) - 4\tilde{h}^{224}(k) \right), \\ S^1(k) &= 2 - \frac{2}{5}\rho \left(2\tilde{h}^{220}(k) - \tilde{h}^{222}(k) + \frac{16}{3}\tilde{h}^{224}(k) \right), \\ S^2(k) &= 2 - \frac{2}{5}\rho \left(2\tilde{h}^{220}(k) + 2\tilde{h}^{222}(k) - \frac{4}{3}\tilde{h}^{224}(k) \right), \end{aligned} \quad (33)$$

where

$$\tilde{h}^{22l}(k) = 4\pi i^l \int_0^\infty j_l(kr) h^{22l}(r) r^2 dr. \quad (34)$$

In Eq. (34), $\tilde{h}^{mnl}(k)$ is the Hankel transform of the projection $h^{mnl}(r)$ of the solvent-solvent pair correlation function on the corresponding rotational invariant,⁵⁹ $j_l(x)$ is the spherical Bessel function.⁶⁰

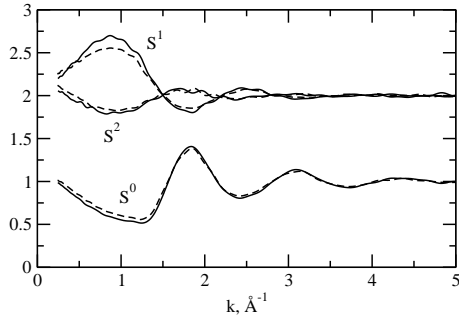


FIG. 4: Quadrupolar structure factors for the 12-site (rigid, nonpolarizable) benzene;⁶¹ $T = 298$ K (solid lines) and $T = 342$ K (dashed lines).

Equations (32) were applied to calculate $S^m(k)$ from NVT MC simulations with varying quadrupole moment ($(Q^*)^2 = (0.1, 0.3, 0.5)$ in Fig. 3a). It turns out that the three quadrupolar structure factors can approximately be brought to one master curve by proper rescaling (Fig. 3b). This observation indicates that the long-range projection $\tilde{h}^{224}(k)$ is the main component of $S^m(k)$ suggesting a simple perturbation approach to the calculation of $S^m(k)$. Taking the liquid without the quadrupolar interactions as a reference we expand $\tilde{h}^{224}(k)$ in the quadrupole-quadrupole interaction potential truncating the expansion by the first order term. Equation (33) can then be re-written in terms of the two-particle (super-script “(2)”) perturbation integral as follows

$$\begin{aligned} S^0(k) &= 1 - 12y_q I^{(2)}(k\sigma, \rho^*), \\ S^1(k) &= 2 + 16y_q I^{(2)}(k\sigma, \rho^*), \\ S^2(k) &= 2 - 4y_q I^{(2)}(k\sigma, \rho^*), \end{aligned} \quad (35)$$

where

$$y_q = \frac{2\pi}{5} \beta \rho Q^2 / \sigma^2 \quad (36)$$

is the reduced density of solvent quadrupoles⁵ and σ is the hard-sphere diameter. Note that the next perturbation term will result in the three-particle perturbation integral which we do not consider here. An improvement of the present description can be sought in terms of a Padé-truncated⁴⁸ perturbation expansion for $S^m(k)$.

The perturbation integral in Eq. (35)

$$I^{(2)}(k\sigma, \rho^*) = \int_1^\infty dx g_{ss}^{(0)}(x, \rho^*) j_4(k\sigma x) / x^3 \quad (37)$$

is defined in terms of the fourth order spherical Bessel function, $j_4(x)$, and the solvent-solvent radial distribution function $g_{ss}^{(0)}(x, \rho^*)$, where $x = r/\sigma$. For a fluid of

TABLE I: Third-order polynomials $a_n(\rho^*)$ in reduced density ρ^* used in Eqs. (38) and (39).

p	$a_{1,p}$	$a_{2,p}$	$a_{3,p}$	$a_{4,p}$
0	0.0095	0.0901	0.0971	0.0620
1	-0.0776	0.3580	-0.4647	0.5574
2	0.0800	-0.5657	1.0580	-0.7940
3	0.0123	0.1290	-0.4370	0.4810

hard-sphere quadrupoles, the perturbation integral depends on $k\sigma$ and the reduced solvent density ρ^* . It can be approximated by a series of spherical Bessel functions:

$$I^{(2)}(k\sigma, \rho^*) = \sum_{n=1}^4 a_n(\rho^*) j_n(k\sigma), \quad (38)$$

where each $a_n(\rho^*)$ is a third-order polynomial in reduced density:

$$a_n(\rho^*) = \sum_{p=0}^3 a_{n,p}(\rho^*)^p. \quad (39)$$

The fitting coefficients $a_{n,p}$ obtained by using the corrected Percus-Yevick radial distribution function for hard sphere fluids⁶² are listed in Table I. The fit covers the range of reduced densities $\rho^* = 0.5 - 1.0$.

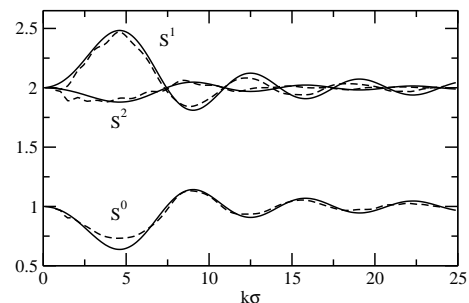


FIG. 5: Quadrupolar structure factors for fluids of hard-sphere axial quadrupoles from the perturbation expansion (Eqs. (35)–(38), solid lines) and from the MC simulations (dashed lines); $\rho^* = 0.8$ and $(Q^*)^2 = 0.3$.

The analytical equations for the structure factors [Eqs. (35)–(38)] are compared to MC simulation results for the fluid of hard-sphere axial quadrupoles in Fig. 5. The agreement is particularly good for $(Q^*)^2 \leq 0.3$. Equations (35)–(38) are also used to define the structure factors of the 12-site model of benzene (Fig. 2) approximated by the axial quadrupole with the magnitude given by Eq. (22). A reasonable agreement is obtained even by using the hard sphere radial distribution function instead of the actual pair distribution function of the reference potential of benzene (Fig. 6).

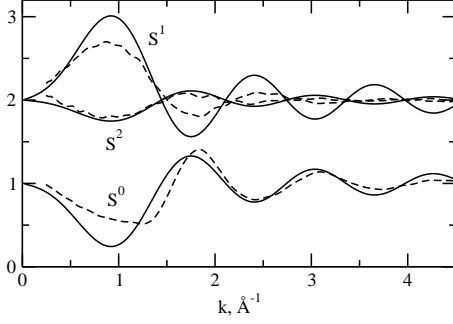


FIG. 6: Quadrupolar structure factors for the 12-site benzene from the perturbation expansion (Eqs. (35)–(38), solid lines) and from the MD simulations (dashed lines); $T=298$ K, $\rho^* = 0.982$, and $(Q^*)^2 = 0.45$.

V. MODEL SYSTEMS

The theory is first tested on two model solutes serving as reference for many solvation studies: spherical ion and spherical dipole, both dissolved in an axial-quadrupole solvent. The formal theory is tested against the MC simulations. Two types of simulations have been carried out. In the first set, we obtain the axial-quadrupole structure factors (Appendix A) required as input to the formal theory [Eq. (30)]. In the second set, we directly calculate the LRA chemical potential of solvation [Eq. (13)] from fluctuations of the solute-solvent potential (Appendix B).

A. Ion

For a point charge q_0 inside a spherical cavity one has $\tilde{\phi}^{1,2}(\mathbf{k}) = 0$ and the only nonzero component is given by

$$\tilde{\phi}^0(\mathbf{k}) = \frac{(4\pi q_0)^2}{5} \frac{j_1^2(kR_{0s})}{(kR_{0s})^2}, \quad (40)$$

where $R_{0s} = (\sigma_0 + \sigma)/2$ is the distance of the closest approach of the solvent (diameter σ) to the solute (diameter σ_0). Equations (30) and (31) then yield

$$-\beta\mu_{0s} = y_q (q_0^*)^2 [I^Q(r_{0s}, \rho^*, y_q) + I^D(r_{0s}, \rho^*, y_q)], \quad (41)$$

where $(q_0^*)^2 = \beta q_0^2/\sigma$. The perturbation integrals in Eq. (41) are

$$\begin{aligned} I^Q(r_{0s}, \rho^*, y_q) &= \frac{2}{\pi r_{0s}^4} \int_0^\infty dx j_1^2(xr_{0s}) S^0(x), \\ I^D(r_{0s}, \rho^*, y_q) &= \int_{r_{0s}}^\infty \frac{h_{0s}^{(0)}(x) dx}{x^4}. \end{aligned} \quad (42)$$

The perturbation integrals depend on the solvent reduced density $\rho^* = \rho\sigma^3$, the solvent quadrupolar density y_q [Eq. (36)], and the solute-solvent size ratio $r_{0s} = R_{0s}/\sigma$. They are tabulated as polynomials of ρ^* and $1/r_{0s}$ in Sec. V C.

Equation (41) is the microscopic perturbation solution for solvation of an ion. Below we will also consider two

approximations to the complete solution: continuum approximation and single-particle approximation. The continuum limit for the solvation chemical potential can be obtained from the microscopic formulation by assuming that $\tilde{\phi}^0(k)$ changes much faster as a function of k than does the structure factor $S^0(k)$. When this is true, one can put $S^0(k) \simeq S^0(0)$ in Eq. (42). The density component disappears in the continuum limit⁵⁰ with the final result

$$-\beta\mu_{0s}^C = y_q S^0(0) \frac{(q_0^*)^2}{3r_{0s}^3}, \quad (43)$$

where the superscript ‘‘C’’ refers to the continuum limit. When correlations between the solvent dipoles are neglected by assuming $\tilde{h}^{22l} = 0$ one gets ($S^0(0) = 1$)

$$-\beta\mu_{0s}^S = y_q \frac{(q_0^*)^2}{3r_{0s}^3}, \quad (44)$$

where the superscript ‘‘S’’ refers to the single-particle approximation.

B. Dipole

For a solute represented by a point dipole \mathbf{m}_0 at the center of a spherical cavity of diameter σ_0 , $\tilde{\phi}^2(\mathbf{k}) = 0$, and two other components are

$$\tilde{\phi}^0(\mathbf{k}) = (4\pi)^2 \frac{9(\mathbf{m}_0 \cdot \hat{\mathbf{k}})^2}{5} \frac{j_2^2(kR_{0s})}{(kR_{0s})^2}, \quad (45)$$

$$\tilde{\phi}^1(\mathbf{k}) = (4\pi)^2 \frac{3(m_0^2 - (\mathbf{m}_0 \cdot \hat{\mathbf{k}})^2)}{10} \frac{j_2^2(kR_{0s})}{(kR_{0s})^2}.$$

The total solvation chemical potential becomes

$$-\beta\mu_{0s} = y_q (m_0^*)^2 [I^Q(r_{0s}, \rho^*, y_q) + I^D(r_{0s}, \rho^*, y_q)], \quad (46)$$

where $(m_0^*)^2 = \beta m_0^2/\sigma^3$ and the perturbation integrals are

$$\begin{aligned} I^Q(r_{0s}, \rho^*, y_q) &= \frac{2}{\pi r_{0s}^4} \int_0^\infty dx j_2^2(xr_{0s}) (3S^0(x) + S^1(x)), \\ I^D(r_{0s}, \rho^*, y_q) &= 5 \int_{r_{0s}}^\infty \frac{h_{0s}^{(0)}(x) dx}{x^6}. \end{aligned} \quad (47)$$

A polynomial approximation for dipolar $I^{Q,D}(r_{0s}, \rho^*, y_q)$ is given in Sec. V C.

The continuum and single-particle limits for dipolar solvation are

$$-\beta\mu_{0s}^C = y_q [3S^0(0) + S^1(0)] \frac{(m_0^*)^2}{5r_{0s}^5} \quad (48)$$

and

$$-\beta\mu_{0s}^S = y_q \frac{(m_0^*)^2}{r_{0s}^5}. \quad (49)$$

C. Perturbation integrals for μ_{0s}^Q

Algebraic expressions for integrals $I^Q(r_{0s}, \rho^*, y_q)$ in Eqs. (42) and (47) can be obtained by using the perturbation expansion for the quadrupolar structure factors in Eq. (35). The following integrals need to be calculated:

$$\int_0^\infty dx j_1^2(xr_{0s})j_4(xy) = \begin{cases} \frac{\pi y}{1536r_{0s}^4}(8r_{0s}^2 + y^2), & 2r_{0s} \geq y \\ \frac{\pi}{12y^5}(5r_{0s}^2y^2 - 14r_{0s}^4), & 2r_{0s} < y \end{cases} \quad (50)$$

and

$$\int_0^\infty dx j_2^2(xr_{0s})j_4(xy) = \begin{cases} \frac{\pi y}{15360r_{0s}^6}(80r_{0s}^4 + 30r_{0s}^2y^2 - 9y^4), & 2r_{0s} > y \\ \frac{7\pi r_{0s}^4}{30y^5}, & 2r_{0s} < y, \end{cases} \quad (51)$$

where $x = k\sigma$ and $y = r/\sigma$.

The perturbation integral $I^Q(r_{0s}, \rho^*, y_q)$ in Eq. (42) is then

$$I^Q(r_{0s}, \rho^*, y_q) = \frac{1}{3r_{0s}^3} + y_q I_{\text{ion}}(r_{0s}, \rho^*), \quad (52)$$

where

$$I_{\text{ion}}(r_{0s}, \rho^*) = 28r_{0s}^2 I_{2,8}(r_{0s}, \rho^*) - 10I_{2,6}(r_{0s}, \rho^*) - \frac{1}{8r_{0s}^4} I_{1,-2}(r_{0s}, \rho^*) - \frac{1}{64r_{0s}^6} I_{1,0}(r_{0s}, \rho^*). \quad (53)$$

Similarly, $I^Q(r_{0s}, \rho^*, y_q)$ for the dipolar solute in Eq. (47) is

$$I^Q(r_{0s}, \rho^*, y_q) = \frac{1}{r_{0s}^5} + y_q I_{\text{dipole}}(r_{0s}, \rho^*), \quad (54)$$

where

$$I_{\text{dipole}}(r_{0s}, \rho^*) = -\frac{28}{3} I_{2,8}(r_{0s}, \rho^*) - \frac{5}{24r_{0s}^6} I_{1,-2}(r_{0s}, \rho^*) - \frac{5}{64r_{0s}^8} I_{1,0}(r_{0s}, \rho^*) - \frac{3}{128r_{0s}^{10}} I_{2,2}(r_{0s}, \rho^*). \quad (55)$$

In Eqs. (53) and (55),

$$I_{1,n}(r_{0s}, \rho^*) = \int_1^{2r_{0s}} dx g_{ss}^{(0)}(x, \rho^*) x^n, \quad (56)$$

and

$$I_{2,n}(r_{0s}, \rho^*) = \int_{2r_{0s}}^\infty dx \frac{g_{ss}^{(0)}(x, \rho^*)}{x^n}. \quad (57)$$

The numerical values of the perturbation integrals in Eqs. (53) and (55) were fit to polynomials in ρ^* and $1/r_{0s}$ as follows

$$I_{\text{ion}}(r_{0s}, \rho^*) = \sum_{n=4}^{11} \frac{a_n(\rho^*)}{r_{0s}^n}, \quad (58)$$

$$I_{\text{dipole}}(r_{0s}, \rho^*) = \sum_{n=6, n \neq 9}^{14} \frac{a_n(\rho^*)}{r_{0s}^n}, \quad (59)$$

where $a_n(\rho^*)$ are third-order polynomials in ρ^* :

$$a_n(\rho^*) = \sum_{p=0}^3 a_{n,p}(\rho^*)^p. \quad (60)$$

The fit covers ρ^* ranging from 0.5 to 1.0 and r_{0s} ranging from 0.8 to 2.4; the coefficients a_n are listed in Table II.

D. Comparison to MC results

MC simulations of solvation of spherical ions and dipoles have been carried out to test the formal theory. A solute is chosen as a hard sphere, $\sigma_0/\sigma = 1.8$, with charge, $(q_0^*)^2 = \beta q_0^2/\sigma = 15$, or with point dipole, $(m_0^*)^2 = \beta m_0^2/\sigma^3 = 15$, at the center. The initial configuration in the cubic simulation box is created to accommodate the solute at its center and N solvent molecules with their size adjusted to keep $\rho^* = 0.8$. The details of reaction-field and Ewald sum corrections for the solute-solvent and solvent-solvent interaction potentials are given in Appendix B.

The results for solvation of the ionic solute are listed in Tab. III. Columns 2–4 give the variance of the the solute-solvent interaction potential from simulations. Simulations of ion solvation at $N = 256, 500$, and 864 show a noticeable size effect. Therefore, the infinite-dilution result (column 5) was obtained by extrapolating the data at various N to $N \rightarrow \infty$. Column 6 gives the theoretical μ_{0s} . Its separation into the quadrupolar orientational component, μ_{0s}^Q , and the density component, μ_{0s}^D , is given in columns 7 and 8, respectively. The single-particle response μ_{0s}^S (column 9) turns out to be surprisingly close to μ_{0s} from MC simulations.

Results for solvation of the point hard-sphere dipole are shown in Tab. IV. No dependence of the calculated quantities on the system size has been observed in this case for $N \geq 500$. Columns 2 and 3 give the average of the solute-solvent interaction energy and its variance. The near equality of these numbers supports the use of the LRA.⁴⁵ Column 5 gives the orientational part μ_{0s}^Q from Eq. (46). This component is about half of the overall solvation chemical potential as is seen from the comparison of column 5 to columns 2 and 3. The density component μ_{0s}^D from Eq. (46) adds to μ_{0s}^Q to give the total μ_{0s} in column 4 which is uniformly higher than the results of MC simulations.

TABLE II: Perturbation integrals from Eqs. (58)–(60). Numbers in columns indicate the coefficients b_{np} in Eq. (60).

I_{ion}								
p	$a_{4,p}$	$a_{5,p}$	$a_{6,p}$	$a_{7,p}$	$a_{8,p}$	$a_{9,p}$	$a_{10,p}$	$a_{11,p}$
0	-1/8	0.061	1/64	-1.341	4.284	-5.611	3.39	-0.777
1	1.618	-15.631	59.278	-118.0	132.458	-83.681	27.214	-3.447
2	-5.240	49.322	-190.549	393.41	-469.0	323.172	-119.348	18.254
3	3.508	-33.3	130.4	-274.236	334.8	-237.6	90.924	-14.506
I_{dipole}								
p	$a_{6,p}$	$a_{7,p}$	$a_{8,p}$	$a_{10,p}$	$a_{11,p}$	$a_{12,p}$	$a_{13,p}$	$a_{14,p}$
0	-5/24	-1/8	5/64	1/128	3.781	-8.604	6.739	-1.8
1	-1.615	11.195	-23.650	87.281	-179.677	176.884	-88.443	17.9
2	4.530	-32.342	70.892	-268.563	531.415	-492.183	229.817	-43.5
3	-2.614	18.942	-42.622	167.772	-333.548	307.841	-142.424	26.614

TABLE III: Formal theory and MC results for ionic solute.

$(Q^*)^2$	$N = 256$	500	864	∞	$-\beta\mu_{0s}^b$	$-\beta\mu_{0s}^Q{}^b$	$-\beta\mu_{0s}^D{}^b$	$-\beta\mu_{0s}^S{}^c$
		$\beta^2\langle\delta v_{0s}^2\rangle/2^a$						
0.1	0.23	0.24	0.24	0.26	0.30	0.18	0.12	0.18
0.2	0.42	0.87	0.44	0.48	0.60	0.35	0.25	0.37
0.3	0.59	0.60	0.61	0.65	0.86	0.49	0.37	0.55
0.4	0.73	0.76	0.77	0.84	1.12	0.63	0.49	0.73
0.5	0.87	0.89	0.91	1.00	1.36	0.74	0.62	0.92
0.6	0.99	1.02	1.04	1.15	1.60	0.88	0.72	1.10

^aMC simulations.^bEq. (41).^cSingle-particle solution, Eq. (44).

In order to pin down the origin of the overestimated values, we compare our results with the Padé form of the perturbation expansion for a point dipole solute⁵ (column 7). This latter solution, which is in overall good agreement with simulations, can also be split into the orientational and density components (columns 8 and 9). The comparison of the orientational components of μ_{0s} in columns 5 and 8 and the density components in columns 6 and 9 shows that it is the latter part that is overestimated in the calculation based on Eq. (31). Finally, the single-particle estimate, μ_{0s}^S (column 10), compares well with μ_{0s}^Q obtained from the quadrupolar structure factors (cf. columns 5 and 10). The relatively high weight of the density component in dipole solvation makes the single-particle approximation less reliable than in the case of ion solvation. However, in overall, the single-particle formula works well for quadrupolar solvation. This observation is consistent with the earlier notion by Ladanyi and Maroncelli³ that the collective nature of the solvation response diminishes for higher multipoles and that non-dipolar solvation is dominated by single-particle response. We also note that the use of the quadrupolar structure factors from the analytical equations [Eqs. (35)–(38)] gives results nearly identical (deviation $\leq 1\%$) to the values obtained with simulated structure factors.

VI. COMPARISON TO EXPERIMENT

In this section we apply the present model to the calculation of ET rates in the donor-acceptor complex shown in Fig. 1. The density component of μ_{0s} is hard to estimate for a molecule of such complex shape. On the other hand the charge in the charge-separated state D^+BA^- is located close to the molecular surface. One might then expect that the solute-solvent interaction is locally of the ion-quadrupole type. Our calculations in Sec. IV show that for this type of interaction potential the orientational part constitutes about 75% of the overall solvation energy. The calculations below thus assume only the orientational component present in the solvent response

$$\mu_{0s} \simeq \mu_{0s}^Q. \quad (61)$$

A. Free energy gap and the reorganization energy

Forward, $k_{\text{for}}(T)$, and backward, $k_{\text{back}}(T)$, rates are available for complex **1** in benzene,^{65,66} whereas only forward rates have been measured in acetonitrile.⁶⁷ Rate measurements in benzene at different temperatures give access to the overall reaction free energy

$$-\beta\Delta_r G(T) = \ln(k_{\text{for}}(T)/k_{\text{back}}(T)). \quad (62)$$

TABLE IV: Formal theory and MC results for dipolar solute.

$(Q^*)^2$	$-\beta \langle v_{0s} \rangle / 2^a$	$\beta^2 \langle \delta v_{0s}^2 \rangle / 2^a$	$-\beta \mu_{0s}^b$	$-\beta \mu_{0s}^Q{}^b$	$-\beta \mu_{0s}^D{}^b$	$-\beta \mu_{0s}^c$	$-\beta \mu_{0s}^Q{}^c$	$-\beta \mu_{0s}^D{}^c$	$-\beta \mu_{0s}^S{}^d$
0.1	0.59	0.52	0.52	0.26	0.26	0.51	0.27	0.24	0.28
0.2	1.07	0.99	1.05	0.52	0.53	0.96	0.53	0.44	0.56
0.3	1.48	1.41	1.56	0.77	0.79	1.38	0.78	0.60	0.84
0.4	1.91	1.83	2.06	1.00	1.06	1.75	1.02	0.73	1.12
0.5	2.24	2.19	2.56	1.24	1.32	2.10	1.25	0.84	1.40
0.6	2.60	2.53	3.04	1.46	1.58	2.40	1.46	0.93	1.68

^aMC simulations.

^bEq. (46).

^cPadé approximant from Ref. 5. The splitting into the orientational and density parts of the solvation energy is achieved by putting $\rho^* = 0$ in the perturbation integrals when the orientational part is evaluated.

^dSingle-particle solution, Eq. (49).

TABLE V: Solvent parameters used in the calculations.

Solvent	ϵ_s	ϵ_∞	σ_s^a , Å	α , Å ³	m , D	Q	η	ϵ_{ss}^b
Benzene ^c	1.00	1.00	5.28	10.0	0.	8.63	0.520	544
Benzene	2.24	2.24	5.28	10.4	0.	8.35 ^d	0.515 ^a	544
Acetonitrile	35.0	1.80	4.14	4.48	3.9	2.49 ^d	0.424 ^a	100

^aFrom Ref. 63.

^bIn K, from Ref. 64.

^cParameters of the model benzene used in calculations.

^dIn D×Å, from Ref. 2.

The free energy gap is a composite quantity including the vacuum energy gap $\Delta_{\text{vac}}G$, the quadrupolar free energy Δ_qG , the free energy of solvation by induced solvent dipoles $\Delta_{\text{ind}}G$, and the dispersion free energy $\Delta_{\text{disp}}G$:

$$\Delta_rG = \Delta_{\text{vac}}G + \Delta_qG + \Delta_{\text{ind}}G + \Delta_{\text{disp}}G. \quad (63)$$

The difference in free energies is taken between the charge-separated final state (“f”, D^+BA^-) and the initial state (“i”, D^*BA) created by photoexcitation of the anthracene moiety of the donor.^{65,66,67}

The quadrupolar component of the energy gap is the difference of the final and initial values of the chemical potential of solvation

$$\Delta_qG = \mu_{0s}^f - \mu_{0s}^i. \quad (64)$$

Using Eq. (30), Eq. (64) can be re-written as follows

$$\Delta_qG = -\frac{\beta\rho Q^2}{4\pi^2} \sum_m \int_0^\infty dk (f_f^m(k) - f_i^m(k)) S^m(k), \quad (65)$$

where

$$f_{i,f}^m(k) = k^2 \langle \tilde{\phi}_{i,f}^m(\mathbf{k}) \rangle_{\mathbf{k}}. \quad (66)$$

The functions $f_{i,f}^m(k)$ are shown in Fig. 7 (“i” in (a) and “f” in (b)).

The induction solvation is caused by the interaction of an induced solvent dipoles at point \mathbf{r} with the elec-

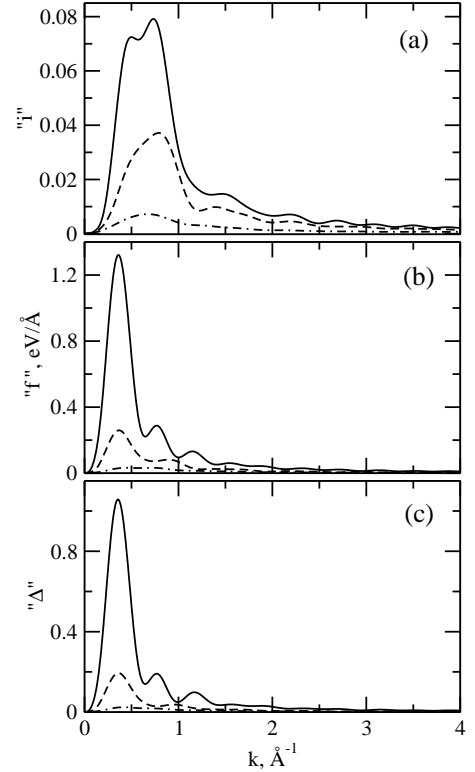


FIG. 7: Rotational projections $f_{i,f,\Delta}^m$ from Eqs. (66) and (78) calculated for complex **1**: $m = 0$ (solid lines), $m = 1$ (dashed lines), and $m = 2$ (dash-dotted lines). Calculations are carried out for the charge distribution in the initial (“i”) D^*BA state (a), final (“f”) D^+BA^- state (b), and with the atomic charge distribution obtained as difference (“ Δ ”) of the atomic charges in the final and initial states (c).

tric field of the solute. The free energy of induction solvation is obtained by integrating the real-space electrostatic energy density $E_{i,f}(\mathbf{r})^2$ with the distribution function $g_{0s}(\mathbf{r})$ of the solvent molecules around the solute

$$\Delta_{\text{ind}}G = -(\rho\alpha/2) \int g_{0s}(\mathbf{r}) [E_f(\mathbf{r})^2 - E_i(\mathbf{r})^2] d\mathbf{r}. \quad (67)$$

As in the case of quadrupolar solvation, we will neglect the solute solvent correlation function replacing $g_{0s}(\mathbf{r})$ with a step function $\theta(\mathbf{r})$ which is equal to zero within the solute and is equal to one otherwise. By defining the Fourier transform of the electric field according to the relation

$$\tilde{\mathbf{E}}(\mathbf{k}) = \int \mathbf{E}(\mathbf{r})\theta(\mathbf{r})e^{i\mathbf{k}\cdot\mathbf{r}}d\mathbf{r} \quad (68)$$

one can rewrite Eq. (67) in the form of one-dimensional k -integral

$$\Delta_{\text{ind}}G = -\frac{\rho\alpha}{4\pi^2} \int_0^\infty dk k^2 (\mathcal{E}_f(k) - \mathcal{E}_i(k)). \quad (69)$$

Here, the density of electrostatic energy $\mathcal{E}(k) = \mathcal{E}^L(k) + \mathcal{E}^T(k)$ can be separated into its longitudinal and transverse components:

$$\begin{aligned} \mathcal{E}^L(k) &= \langle |(\tilde{\mathbf{E}}(\mathbf{k}) \cdot \hat{\mathbf{k}})|^2 \rangle_{\mathbf{k}} \\ \mathcal{E}^T(k) &= \langle |\tilde{\mathbf{E}}(\mathbf{k})|^2 \rangle_{\mathbf{k}} - \mathcal{E}^L(k). \end{aligned} \quad (70)$$

The functions $k^2\mathcal{E}^{L,T}(k)$ are shown in Fig. 8.

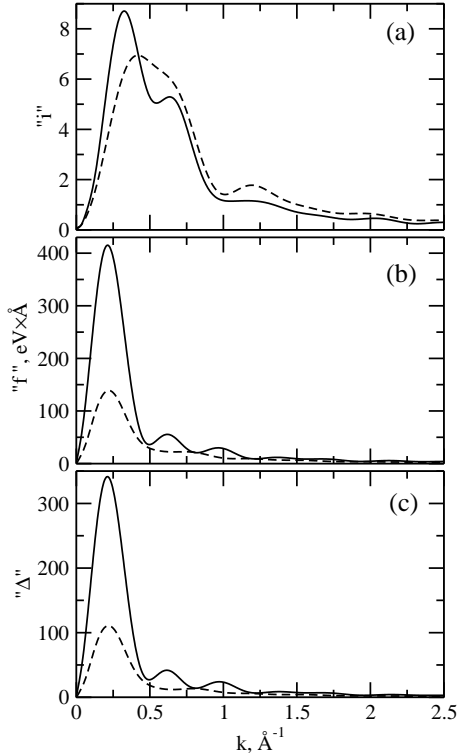


FIG. 8: Longitudinal (solid lines) and transverse (dashed lines) projections of the electrostatic energy density [Eq. (70)] calculated for complex **1**. (a) refers to the initial (“i”) state, (b) refers to the final (“f”) state, (c) corresponds to the solute charge density obtained as difference (“Δ”) in atomic charges in the final and initial states [Eq. (75)].

The dispersion component $\Delta_{\text{disp}}G$ is determined as the change in the total LJ solute-solvent interaction energy

integrated over the solvent volume Ω

$$\Delta_{\text{disp}}G = \rho \int_{\Omega} \Delta u_{LJ}(\mathbf{r})d\mathbf{r}. \quad (71)$$

Here

$$u_{LJ}(\mathbf{r}) = 4 \sum_a \varepsilon_{as} \left[\left(\frac{\sigma_{as}}{|\mathbf{r} - \mathbf{r}_0^a|} \right)^{12} - \left(\frac{\sigma_{as}}{|\mathbf{r} - \mathbf{r}_0^a|} \right)^6 \right], \quad (72)$$

$\varepsilon_{as} = \sqrt{\varepsilon_0^a \varepsilon_s}$ and $\sigma_{as} = (\sigma_0^a + \sigma)/2$. The sum in Eq. (72) runs over all atoms in the solute. The atomic diameters, σ_0^a , and LJ energies, ε_0^a , are parametrized with the OPLS.⁶⁸ The solvent parameters are listed in Table V.

Calculations in acetonitrile were done without the quadrupolar component in the reaction free energy gap because of the very small reduced quadrupole moment of acetonitrile Q^* relative to its reduced dipole m^* (see Table V)⁶⁹

$$\Delta_r G = \Delta_{\text{vac}}G + \Delta_p G + \Delta_{\text{disp}}G. \quad (73)$$

The dipolar component, $\Delta_p G$, is calculated from the formalism developed in Ref. 37 based on the integration of the longitudinal, $\chi^L(k)$, and transverse, $\chi^T(k)$, components of the dipolar response function with the solute electric field:

$$\Delta_p G = -\frac{1}{2} \int \frac{d\mathbf{k}}{(2\pi)^3} \sum_{P=L,T} \chi^P(\mathbf{k})\mathcal{E}^P(\mathbf{k}). \quad (74)$$

The reorganization energy of polar solvation λ_p is defined on the difference electric field $\tilde{\mathbf{E}}_{\Delta} = \tilde{\mathbf{E}}_f - \tilde{\mathbf{E}}_i$. The electrostatic energy density

$$\mathcal{E}_{\Delta}(\mathbf{k}) = \left| \tilde{\mathbf{E}}_{\Delta}(\mathbf{k}) \right|^2 \quad (75)$$

then separates into the longitudinal and transverse components resulting in corresponding components of the reorganization energy

$$\lambda_p = \frac{1}{2} \int \frac{d\mathbf{k}}{(2\pi)^3} \sum_{P=L,T} \chi_n^P(k)\mathcal{E}_{\Delta}^P(\mathbf{k}). \quad (76)$$

In Eq. (76), $\chi_n^{L,T}(\mathbf{k})$ are the nuclear response functions which, in contrast to $\chi^{L,T}(\mathbf{k})$, do not contain the effect of induced solvent dipoles.^{37,38}

The reorganization energy of quadrupolar solvation λ_q is given in terms of the gradient of $\mathbf{E}_{\Delta}(\mathbf{k})$. Following our formal derivation in terms of spherical coordinates, the final result can be written as

$$\lambda_q = \frac{\beta\rho Q^2}{4\pi^2} \sum_m \int dk f_{\Delta}^m(k)S^m(k), \quad (77)$$

where

$$f_{\Delta}^m(k) = k^2 \langle \tilde{\phi}_{\Delta}^m(\mathbf{k}) \rangle_{\mathbf{k}} \quad (78)$$

and $\tilde{\phi}_{\Delta}^m(\mathbf{k})$ is obtained from the solute charge distribution build on difference atomic charges in the final and initial states (Fig. 7c).

TABLE VI: Thermodynamics parameters (eV) of equilibrium solvation of complex **1** in benzene.

T/K	$\Delta_q G^a$	$\Delta_q G^b$	$\Delta_{\text{ind}} G$	$\Delta_{\text{disp}} G^c$	$\Delta_{\text{disp}} G^d$	$\Delta_r G^e$	$\Delta_r G^f$	$\Delta_r G^g$	λ_q^a	λ_q^b
298	-0.244	-0.236	-0.322	0.196	0.460	-0.113	-0.106	-0.110 ^h	0.205	0.198
312	-0.226	-0.221	-0.317	0.193	0.453	-0.092	-0.090	-0.097	0.189	0.185
326	-0.218	-0.208	-0.312	0.190	0.446	-0.082	-0.085	-0.082	0.183	0.174
342	-0.203	-0.196	-0.307	0.186	0.438	-0.066	-0.072	-0.065	0.170	0.164

^aEqs. (65) and (77) with $S^{0,1,2}(k)$ from MD simulations.

^bEqs. (65) and (77) with $S^{0,1,2}(k)$ from Eqs. (35) and (38).

^cCalculated with $\Delta\alpha = 7.22 \text{ \AA}^3$.

^dCalculated with $\Delta\alpha = 17 \text{ \AA}^3$.

^eCalculated with $\Delta\alpha = 7.22 \text{ \AA}^3$ and $\Delta_{\text{vac}} G = 0.258 \text{ eV}$.

^fCalculated with $\Delta\alpha = 17 \text{ \AA}^3$ and $\Delta_{\text{vac}} G = -0.68 \times 10^{-3} \text{ eV}$.

^gExperiment from Eq. (62).

^hCorresponds to $T=296 \text{ K}$.

B. ET rates

The calculations according to the formalism outlined above require the combination of two input components, from the solute and from the solvent. The solute requires specifying coordinates, van der Waals radii (OPLS parameterization⁶⁸), and charges of the solute atoms. The volume accessible to the solvent is limited by the solvent accessible surface (SAS) defined by complementing the solute atomic radii with the half of the solvent hard-sphere diameter, $(\sigma_0^+ + \sigma)/2$. Atomic coordinates and charges for complex **1** (Fig. 1) are from Ref. 70. The Fourier transforms of the solute field and solute field gradient are carried out on the 256^3 grid as described in Appendix D.

The calculation of the dispersion component $\Delta_{\text{disp}} G$ requires knowledge of the alteration of the solute LJ energy with electronic transition. Since this information is not available, we use the London dispersion potential

to connect the change in the LJ energy to the change in the dipolar polarizability. The initial ET state is experimentally produced by photoexcitation of the anthracene moiety of the donor. Anthracene polarizabilities in the ground (subscript “g”) and excited (subscript “e”) states are⁷¹ $\alpha_g = 25 \text{ \AA}^3$ and $\alpha_e = 42 \text{ \AA}^3$. According to the London equation $\varepsilon_{g/e}^a \sim \alpha_{g/e}^2$ (“a” refers to an atomic site within the solute). The LJ energies on the anthracene atoms might hence be expected to scale as $\varepsilon_e^a = (\alpha_e/\alpha_g)^2 \varepsilon_g^a$ leading to the scaling of the solute-solvent dispersion interaction potential as α_e/α_g . In the calculations below we will assume that LJ energies on only the anthracene moiety change with the transition. Since the anion acceptor state of complex **1** might involve some unknown polarizability change off-setting the polarizability change of the anthracene moiety, we consider $\Delta\alpha = \alpha_e - \alpha_g$ as a fitting parameter to reproduce the experimental $\Delta_r G(T)$ [Eq. (62)]. The other fitting parameter is $\Delta_{\text{vac}} G$.

The second input to our calculation formalism comes from properties of the pure solvent. The polar, quadrupolar and dipolar, response comes into the theory in the form of three quadrupolar structure factors $S^m(k)$ and two dipolar structure factors $S^{L,T}(k)$. A parameterization scheme based on solvent dipole moment m , solvent diameter σ , solvent polarizability α , and solvent number density ρ was developed previously in Refs. 37 and 38. Solvent parameters used in the calculation are listed in Table V.

The results of calculation of $\Delta_r G(T)$ and $\lambda_q(T)$ in benzene are listed in Tab. VI. Data in columns 2 and 10 in Table VI have been calculated by using $S^m(k)$ from MD simulations (12-site benzene). Equations (35) and (38) provide an alternative analytical route to $S^m(k)$ through the effective linear quadrupole moment with its magnitude given by Eq. (22). Results of using the analytical structure factors in Eqs. (65) and (77) agree well with

corresponding values obtained by using the structure factors from MD simulations (cf. columns 2, 3 and 10, 11 in Table VI).

The reaction entropy $\Delta S^0 = -d\Delta_r G/dT$ is equal to -8.55 k_B when $\Delta\alpha = 17 \text{ \AA}^3$ of anthracene is used to calculate $\Delta_{\text{disp}} G$ (column 6). The fit of experimental $\Delta_r G(T)$ then yields $\Delta_{\text{vac}} G = -0.68 \times 10^{-3} \text{ eV}$. For these parameters, the dispersion and induction solvation entropies almost cancel each other, $\Delta_{\text{ind}} S^0 = -4.06 \text{ k}_B$ (column 4) and $\Delta_{\text{disp}} S^0 = 5.80 \text{ k}_B$ (column 6), making the quadrupolar solvation entropy, $\Delta_q S^0 = -10.29 \text{ k}_B$ (column 2), nearly equal to the experimental reaction entropy. The experimental value $\Delta S^0 = -11.84 \text{ k}_B$ (column 7) can be reproduced by downward scaling of $\Delta\alpha$ to 7.22 \AA^3 leading to $\Delta_{\text{vac}} G = 0.258 \text{ eV}$. The dispersion solvation entropy then scales down to $\Delta_{\text{disp}} S^0 = 2.46 \text{ k}_B$ (column 5).

The parameters $\Delta\alpha$ and $\Delta_{\text{vac}} G$ from the fit of experi-

TABLE VII: Rates (10^8 s^{-1}) of the ET in benzene.

T/K	k_{for}^a	k_{for}^b	k_{for}^c	k_{back}^a	k_{back}^b	k_{back}^c
298	29.8 ^d	28.54	25.07	0.48 ^d	0.32	0.36
312	27.5	26.86	24.64	0.75	0.79	0.79
326	24.6	26.02	24.97	1.31	1.25	1.11
342	21.5	24.52	24.78	2.41	2.45	1.97

^aExperiment from Ref. 66.

^bTheory with $\Delta\alpha=7.22 \text{ \AA}^3$, $\Delta_{\text{vac}}G = 0.258 \text{ eV}$, and $|V| = 8.0 \text{ cm}^{-1}$.

^cTheory with $\Delta\alpha=17 \text{ \AA}^3$, $\Delta_{\text{vac}}G = -0.68 \times 10^{-3} \text{ eV}$, and $|V| = 7.75 \text{ cm}^{-1}$.

^dMeasurement at $T = 296 \text{ K}$.

mental $\Delta_r G(T)$ have been used to calculate ET rates in benzene (Tab. VII) according to the Jornter-Bixon formula (nonadiabatic ET):

$$k_{\text{for/back}}(T) = \frac{|V|^2}{\hbar} \left(\frac{\pi\beta}{\lambda_s} \right)^{1/2} \sum_{n=0}^{\infty} e^{-S} \frac{S^n}{n!} \exp \left(-\frac{\beta(\lambda_s(T) \pm \Delta_r G(T) + n h \nu_v)^2}{4\lambda_s} \right). \quad (79)$$

Here, $S = \lambda_v / h\nu_v$ is the Huang-Rhys factor and “+” and “-” refer to the forward (“for”) and backward (“back”) reaction rates, respectively. The vibrational reorganization energy $\lambda_v = 0.39 \text{ eV}$ and vibrational frequency $h\nu_v = 1410 \text{ cm}^{-1}$ are from Ref. 66. The experimental rates $k_{\text{for/back}}(T)$ are reproduced with the electronic coupling $|V| = 8 \text{ cm}^{-1}$ and $\Delta_r G(T)$ and $\lambda_q(T)$ from our calculations (columns 3 and 6 in Tab. VII, see also Fig. 9).

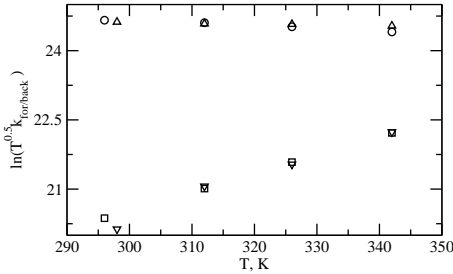


FIG. 9: Forward (circles and up triangles) and backward (squares and down triangles) ET rates in benzene for complex **1**. Triangle symbols correspond to experimental data.⁶⁶ Circles and squares correspond to four temperatures at which $S^{0,1,2}(k)$ have been calculated from MD simulations.

The parameters $\Delta\alpha$ and $\Delta_{\text{vac}}G$ obtained from the fit of $\Delta_r G(T)$ in benzene refer to the solute in the gas phase and do not depend on the solvent. The reliability of our fitting procedure can thus be further tested by using these parameters to calculate ET rates in a different solvent. Since we also want a test independent of the present formulation for quadrupolar solvation, acetonitrile with its small quadrupole moment and large dipole

moment presents an ideal choice. Table VIII lists the calculated thermodynamic parameters and rates of charge separation in complex **1** in acetonitrile in the experimental temperature range between 255 and 335 K.⁶⁷ The calculations of the free energy gap and the reorganization energy are done by using the recently developed microscopic theory of dipolar solvation.^{37,38} The dispersion part of the ET driving force in acetonitrile is calculated according to Eqs.(71) and (72) with the solvent parameters listed in Table V.

TABLE VIII: Free energies (eV) and rate constants (10^8 s^{-1}) for complex **1** in acetonitrile.

T/K	$\Delta_p G$	$\Delta_{\text{disp}} G$	$\Delta_r G$	λ_p	k_{for}
255	-1.739	0.101	-1.381	1.48	2.91
265	-1.688	0.099	-1.331	1.41	3.28
275	-1.640	0.098	-1.285	1.35	3.66
285	-1.597	0.096	-1.243	1.30	4.03
295	-1.557	0.095	-1.204	1.25	4.39
305	-1.513	0.094	-1.161	1.20	4.64
315	-1.485	0.092	-1.134	1.16	5.07
325	-1.452	0.091	-1.103	1.12	5.40
335	-1.422	0.090	-1.074	1.08	5.70

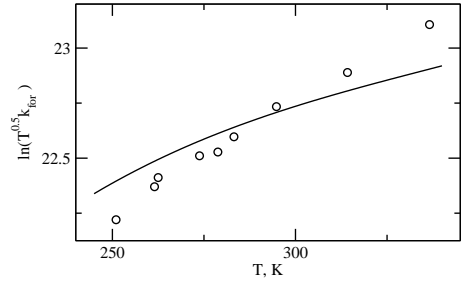


FIG. 10: The forward rates of charge separation in complex **1** in acetonitrile. Open circles refer to experiment, the solid line refers to theory.

Since the electronic coupling may depend on the solvent³⁶ the experimental reaction rates⁶⁷ were fit to Eq. (79) with electronic coupling V considered as the only fitting parameter (Fig. 10). This procedure results in $|V| = 2.21 \text{ cm}^{-1}$. This value is almost 4 times smaller than the corresponding electronic coupling in benzene. This trend parallels the one reported by Zimmt and Waldeck.³⁶ $V = 7.2 \text{ cm}^{-1}$ in benzene vs $V = 4.6 \text{ cm}^{-1}$ in acetonitrile. Qualitatively, this difference is attributed to the higher overlap of the donor and acceptor orbitals of complex **1** with the molecular orbitals of benzene residing in the clamp compared to the molecular orbitals of acetonitrile.³⁶

VII. DISCUSSION

Theories of dipolar solvation have been developed over the last decades to provide a hierarchy of approxima-

TABLE IX: Hierarchy of solutions for the solvation chemical potential, $-\beta\mu_{0s}^Q$, in quadrupolar solvents.

Approximation	Solute	
	Ion	Dipole
Single-particle	$(q_0^*)^2 y_q / 3r_{0s}^3$	$(m_0^*)^2 y_q / r_{0s}^5$
Continuum	$(q_0^*)^2 y_q S^0(0) / 3r_{0s}^3$	$(m_0^*)^2 y_q (3S^0(0) + S^1(0)) / 5r_{0s}^5$
Perturbation	$(q_0^*)^2 y_q (1/3r_{0s}^3 + y_q I_{\text{ion}}(r_{0s}, \rho^*))$	$(m_0^*)^2 y_q (1/r_{0s}^5 + y_q I_{\text{dipole}}(r_{0s}, \rho^*))$
	Arbitrary solute	
Perturbation	$(\beta^2 \rho Q^2 / 2) \sum_m \int \phi^m(\mathbf{k}) S^m(k) d\mathbf{k} / (2\pi)^3$	

tions ranging from the simple estimates of the Born and Onsager equations to more accurate Poisson-Boltzmann equation⁷² and up to microscopic liquid-state calculations in terms of perturbation expansions,^{5,73} integral equations,⁶ or density functional^{74,75} theories. Nothing of comparable scale exists for quadrupolar solvation. Kim and co-workers^{21,22,23,76} have formulated a continuum theory of quadrupolar solvation of spherical solutes. The theory provides a fast calculation formalism, but suffers from the approximation of the spherical solute shape and empirical parameterization of the quadrupolar solvent susceptibility [Eq. (7)]. The integral equation theories of the RISM family^{6,77} avoid the problem of separate calculations of dipolar and quadrupolar solvation by considering the site-site interaction potentials automatically incorporating the infinite-order multipole expansion. This advantage comes at the expense of the necessity to solve rather complex integral equations on

one hand and to supply the charge-charge structure factors of the solvent characterized by its site-site force field on the other. Force field parameterization is available only for a few solvents, and the calculations of the charge-charge structure factors requires extensive computations. Therefore, one would want a formalism for quadrupolar solvation that would incorporate the quadrupole moment of the solvent along with some experimentally available parameters as input in the microscopic solvation formalism. The formulation of such a theory is the result of this paper. It turns out that the quadrupolar structure factors of non-dipolar solvents can indeed be rather accurately calculated based on experimental input parameters for the solvent: quadrupole moment, density, and the effective molecular diameter. Based on these structure factors we have formulated a hierarchy of approximations of increasing sophistication and accuracy listed in Table IX.

As the crudest estimate we offer the single-particle approximation which allows one to calculate the quadrupolar solvation energy from two solvent parameters, the quadrupolar density y_q [Eq. (36)] and the solvent diameter σ . The continuum approximation includes $S^m(0)$. However, since $S^0(0) \simeq 1$ and $S^{1,2}(0) \simeq 2$, the continuum limit is in fact very close to the single-particle result. The next approximation is based on perturbation integrals depending on the reduced solvent density $\rho^* = \rho\sigma^3$ and the reduced distance of the closest solute-solvent approach $r_{0s} = \sigma_0/2\sigma + 0.5$. The number of solvent parameters thus rises to three: y_q , σ , and ρ^* . Finally, the calculation of solvation free energy of a solute of arbitrary shape requires three angular projections of the auto correlation function of quadrupolar polarization (last line in Table IX). The problem which is still remain unresolved is the absence of an accurate algorithm for the density component of the solvation chemical potential μ_{0s}^D [Eqs. (13)]. This component can be included for spherical solutes since the pair solute-solvent spherically symmetric distribution function can be then computed with sufficient accuracy. For instance, in the case of a spherical dipole, the Padé form of perturbation theories⁵ gives a good agreement with simulations.

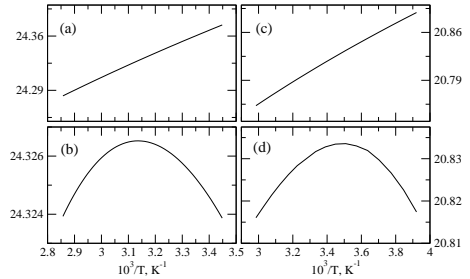


FIG. 11: $\ln(k_{\text{for}})$ vs $1/T$ for complex **1** is calculated in benzene with $\Delta_{\text{vac}}G = 0.173$ eV and in acetonitrile with $\Delta_{\text{vac}}G = 0.19$ eV. In benzene λ_q and $\Delta_r G$: (a) are fixed at $T = 320$ K; (b) assume full temperature dependence. In acetonitrile λ_q and $\Delta_r G$: (c) are fixed at $T = 275$ K; (d) assume full temperature dependence.

Several effective medium approximations have been proposed in the literature to deal with the problem of the local density profile.¹⁰ They replace the solute-solvent interaction potential in the orientational component of the chemical potential of solvation ($v_{0s}\theta(\mathbf{r})$ in Eq. (13)) with an effective solute-solvent coupling including the information about the solute-solvent density correlations (direct

solute-solvent correlation function in the surrogate^{6,10,77} and density functional⁹ theories or vertex in the mode-coupling formulation¹¹). However, all such approximations are heavily dependent on the detailed knowledge of the solute-solvent distribution function which is available only for solutes of simple shape. There is still no acceptable theory adequately addressing the calculation of the μ_{0s}^D components for solutes of complex shape.

The present calculation for complex **1** highlights the importance of the induction and dispersion components of solvation in the equilibrium energy gap of ET reactions (Table VI). The contribution of induction and dispersion forces to the solvent reorganization energy are given, however, by a higher order of the perturbation theory, and they are normally much smaller than the corresponding components of the free energy gap.^{1,78} Quadrupolar solvation then becomes the most significant contribution to the solvent reorganization energy in non-dipolar solvents. In the crudest approximation, the quadrupolar reorganization energy is proportional to the quadrupolar density y_q :

$$\lambda_q \propto q_0^2 \rho \beta Q^2 / (R_0 + \sigma/2)^3 \quad (80)$$

for an ion and

$$\lambda_q \propto m_0^2 \rho \beta Q^2 / (R_0 + \sigma/2)^5 \quad (81)$$

for a dipole. The present theory thus predicts a negative slope of λ_q vs T :

$$(\partial \lambda_q / \partial T)_P \simeq -\lambda_q (T^{-1} + \alpha_P), \quad (82)$$

where α_P is the isobaric volume expansion coefficient. The slope of λ_q vs P is positive and is proportional to isobaric compressibility β_T :

$$(\partial \lambda_q / \partial P)_T \simeq \beta_T \lambda_q. \quad (83)$$

The negative slope of the solvent reorganization energy has been obtained here for both quadrupolar (Table VI) and dipolar (Table VIII) solvents. This property thus seems to be a universal signature of ET reorganization in polar (dipolar and quadrupolar) solvents. This particular dependence of the reorganization energy on temperature results in an observable effect in reactions with low activation barrier as was first noted in Ref. 79. The classical Marcus activation barrier for ET passes through a maximum when plotted vs $1/T$ (Arrhenius plot) at the point of activationless ET $\lambda_{q,p}(T) + \Delta_r G(T) = 0$ when the negative slope of $\lambda_{q,p}$ vs T is applied. Figure 11 illustrates this point by showing $\ln(k_{\text{for}})$ vs $1/T$ calculated on complex **1** for which $\Delta_{\text{vac}} G$ was adjusted to allow the point $\lambda_{q,p}(T) + \Delta_r G(T) = 0$ to fall in the experimental range of temperatures. The calculations with full temperature dependent $\lambda_{q,p}(T)$ and $\Delta_r G(T)$ are compared to the those under assumption $\lambda_{q,p} = \text{Const}$, $\Delta_r G = \text{Const}$. No maximum is seen in the latter case. We note also that intramolecular vibrations tend to mask the appearance of the maximum.

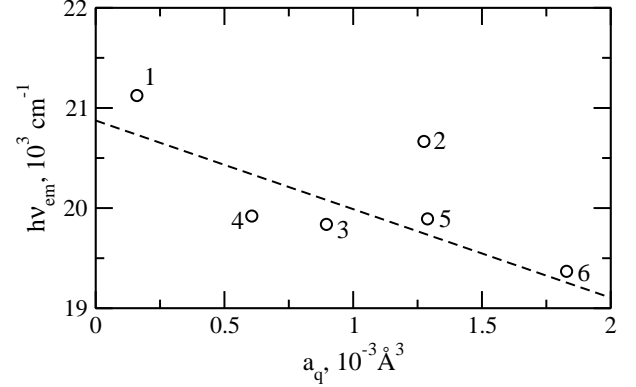


FIG. 12: Emission energy of ADMA⁸⁰ vs a_q [Eq. (85)] in quadrupolar solvents: ethylene (1), CO₂ (2), benzene (3), tetrafluorobenzene (4), toluene (5), 1,4-dioxane (6). Emission energies, solvent parameters, and $R_0 = 4.32 \text{ \AA}$ are taken from Ref. 80. The dashed line is drawn as regression through the solvents excluding CO₂.

Although the full version of the theory is preferable for the analysis of spectroscopy and ET kinetics, the simple single-particle approximation is useful in analyzing the qualitative trends with changing non-dipolar solvent. In particular, quadrupolar solvation results in the solvatochromic shift of optical transitions resulting in the change of chromophore's dipole state $\mathbf{m}_i \rightarrow \mathbf{m}_f$

$$h\Delta\nu_{i \rightarrow f} = -2a_q(\mathbf{m}_f - \mathbf{m}_i) \cdot \mathbf{m}_i, \quad (84)$$

where in the single-particle approximation,

$$a_q = \frac{2\pi\beta\rho Q^2}{5(R_0 + \sigma/2)^5}. \quad (85)$$

Figure 12 illustrates this trend based on the emission energies of ADMA reported by Khajepour and Kauffman.⁸⁰ Note that emission frequencies are affected by dispersion and induction solvation and the deviation of the supercritical CO₂ from the linear trend may be traced to its lower polarizability resulting in lower dispersion and induction stabilization energies.

The present formulation, combined with the previously developed model for dipolar solvation,^{37,38} covers two extreme cases of polar solvation – purely dipolar and purely quadrupolar solvents. The formalism is based on the correlation functions of dipolar and quadrupolar polarization as input and, therefore, can be applied to an arbitrary dipolar or quadrupolar solvent. This approach has allowed us to address the problem of microscopic calculation of solvation thermodynamics for solutes with atomic resolution of geometry and charge distribution. The application to real large donor-acceptor molecules shows encouraging results. Generalization of the theory will require considering dipolar-quadrupolar solvents, which will be a subject of future work.

Acknowledgments

Acknowledgments are made to the donors of The Petroleum Research Fund, administered by the ACS (39539-AC6) for support of this research. We are grateful to Dr. A. Troisi for sharing with us structural data on the cleft molecule and to Prof. M. B. Zimmt and Prof. D. H. Waldeck for the experimental kinetic data.

APPENDIX A: DERIVATION OF EQ. 30.

Here we provide the derivation of the solute field gradient and quadrupolar structure factors in terms of rotationally-invariant contraction of Cartesian tensors. The Cartesian components of Q_{2m} and ϕ_{2m} are

$$\begin{aligned} Q_{20} &= \left(\frac{5}{4\pi}\right)^{1/2} Q_{zz}, \\ Q_{21} &= -\sqrt{\frac{5}{6\pi}}(Q_{xz} + iQ_{yz}), \\ Q_{22} &= \sqrt{\frac{5}{24\pi}}(Q_{xx} - Q_{yy} + 2iQ_{xy}), \end{aligned} \quad (\text{A1})$$

and

$$\begin{aligned} \phi_{20} &= -\sqrt{\frac{\pi}{5}}\phi_{zz}, \\ \phi_{21} &= \sqrt{\frac{4\pi}{30}}(\phi_{xz} + i\phi_{yz}), \\ \phi_{22} &= -\sqrt{\frac{\pi}{30}}(\phi_{xx} - \phi_{yy} + 2i\phi_{xy}). \end{aligned} \quad (\text{A2})$$

Also, for negative $\underline{m} = -m$, $Q_{2,\underline{m}} = (-1)^m Q_{2m}^*$, $\phi_{2,\underline{m}} = (-1)^m \phi_{2m}^*$. For the structure factors in the $X'Y'Z'$ coordinates (\mathbf{k} is collinear to Z' , Fig. 2) one has

$$\begin{aligned} S'^0(k) &= \frac{5}{NQ^2} \left\langle \sum_{i,j} Q'_{zz,i} Q'_{zz,j} e^{i\mathbf{k}\cdot\mathbf{r}_{ij}} \right\rangle, \\ S'^1(k) &= \frac{20}{3NQ^2} \left\langle \sum_{i,j} (Q'_{xz,i} Q'_{xz,j} + Q'_{yz,i} Q'_{yz,j}) e^{i\mathbf{k}\cdot\mathbf{r}_{ij}} \right\rangle, \\ S'^2(k) &= \frac{5}{3NQ^2} \left\langle \sum_{i,j} ((Q'_{xx,i} - Q'_{yy,i})(Q'_{xx,j} - Q'_{yy,j}) + 4Q'_{xy,i} Q'_{xy,j}) e^{i\mathbf{k}\cdot\mathbf{r}_{ij}} \right\rangle. \end{aligned} \quad (\text{A3})$$

Since $\hat{\mathbf{k}}' = (0, 0, 1)$ in $X'Y'Z'$ coordinates and $\mathbf{Q}'_{\alpha\beta}$ is a symmetric and traceless tensors one gets

$$\begin{aligned} Q'_{zz,i} Q'_{zz,j} &= (\hat{\mathbf{k}}' \cdot \mathbf{Q}'_i \cdot \hat{\mathbf{k}}') (\hat{\mathbf{k}}' \cdot \mathbf{Q}'_j \cdot \hat{\mathbf{k}}'), \\ Q'_{xz,i} Q'_{xz,j} + Q'_{yz,i} Q'_{yz,j} &= (\hat{\mathbf{k}}' \cdot \mathbf{Q}'_i \cdot \mathbf{Q}'_j \cdot \hat{\mathbf{k}}') - \\ &\quad (\hat{\mathbf{k}}' \cdot \mathbf{Q}'_i \cdot \hat{\mathbf{k}}') (\hat{\mathbf{k}}' \cdot \mathbf{Q}'_j \cdot \hat{\mathbf{k}}'), \\ (Q'_{xx,i} - Q'_{yy,i})(Q'_{xx,j} - Q'_{yy,j}) + 4Q'_{xy,i} Q'_{xy,j} &= 2\mathbf{Q}'_i : \mathbf{Q}'_j - \\ &\quad 4(\hat{\mathbf{k}}' \cdot \mathbf{Q}'_i \cdot \mathbf{Q}'_j \cdot \hat{\mathbf{k}}') + (\hat{\mathbf{k}}' \cdot \mathbf{Q}'_i \cdot \hat{\mathbf{k}}') (\hat{\mathbf{k}}' \cdot \mathbf{Q}'_j \cdot \hat{\mathbf{k}}'). \end{aligned} \quad (\text{A4})$$

The tensor contractions in Eq. (A4) are invariant under rotations of the coordinate system. Therefore Eq. (A3) can be rewritten as

$$\begin{aligned} S^0(k) &= \frac{5}{NQ^2} \left\langle \sum_{i,j} (\hat{\mathbf{k}} \cdot \mathbf{Q}_i \cdot \hat{\mathbf{k}}) (\hat{\mathbf{k}} \cdot \mathbf{Q}_j \cdot \hat{\mathbf{k}}) e^{i\mathbf{k}\cdot\mathbf{r}_{ij}} \right\rangle, \\ S^1(k) &= \frac{20}{3NQ^2} \left\langle \sum_{i,j} \left[(\hat{\mathbf{k}} \cdot \mathbf{Q}_i \cdot \mathbf{Q}_j \cdot \hat{\mathbf{k}}) - (\hat{\mathbf{k}} \cdot \mathbf{Q}_i \cdot \hat{\mathbf{k}}) (\hat{\mathbf{k}} \cdot \mathbf{Q}_j \cdot \hat{\mathbf{k}}) \right] e^{i\mathbf{k}\cdot\mathbf{r}_{ij}} \right\rangle, \\ S^2(k) &= \frac{5}{3NQ^2} \left\langle \sum_{i,j} \left[2\mathbf{Q}_i : \mathbf{Q}_j - 4(\hat{\mathbf{k}} \cdot \mathbf{Q}_i \cdot \mathbf{Q}_j \cdot \hat{\mathbf{k}}) + (\hat{\mathbf{k}} \cdot \mathbf{Q}_i \cdot \hat{\mathbf{k}}) (\hat{\mathbf{k}} \cdot \mathbf{Q}_j \cdot \hat{\mathbf{k}}) \right] e^{i\mathbf{k}\cdot\mathbf{r}_{ij}} \right\rangle, \end{aligned} \quad (\text{A5})$$

where $\hat{\mathbf{k}} = \mathbf{k}/|\mathbf{k}|$. Also the spherical components $\tilde{\phi}^m(\mathbf{k})$ entering Eq. (30) can be given in the rotation-invariant form as

$$\begin{aligned} \tilde{\phi}^0(\mathbf{k}) &= \frac{1}{20} |(\hat{\mathbf{k}} \cdot \phi \cdot \hat{\mathbf{k}})|^2, \\ \tilde{\phi}^1(\mathbf{k}) &= \frac{1}{30} \left((\hat{\mathbf{k}} \cdot \phi^* \cdot \phi \cdot \hat{\mathbf{k}}) - |(\hat{\mathbf{k}} \cdot \phi \cdot \hat{\mathbf{k}})|^2 \right), \\ \tilde{\phi}^2(\mathbf{k}) &= \frac{1}{120} \left(2\phi^* : \phi - 4(\hat{\mathbf{k}} \cdot \phi^* \cdot \phi \cdot \hat{\mathbf{k}}) + |(\hat{\mathbf{k}} \cdot \phi \cdot \hat{\mathbf{k}})|^2 \right), \end{aligned} \quad (\text{A6})$$

where ϕ stands for $\tilde{\phi}_{\alpha\beta}(\mathbf{k})$. A numerical algorithm for the calculation of $\tilde{\phi}_{\alpha\beta}(\mathbf{k})$ used in the calculations of complex **1** is outlined in Appendix D.

APPENDIX B: DETAILS OF MC SIMULATIONS

1. Quadrupolar hard-sphere fluids

MC simulations have been carried out on a system of $N = 500$ hard sphere molecules with axial quadrupoles placed in a cubic simulation box. Periodic boundary conditions, minimum image convention, and the ratio of 0.5

between the distance of interaction cutoff and the size of the simulation box have been adopted.⁸¹ The cutoff of the quadrupole-quadrupole interactions is corrected by the reaction field of continuum dielectric with the dielectric constant $\epsilon' = \infty$. Simulation runs of the average length of 9×10^5 cycles with 4×10^5 cycles used to calculate $S^m(k)$ were performed at $(Q^*)^2 = \beta\rho Q^2/\sigma^5 = (0.1, 0.2, 0.3, 0.4, 0.5, 0.6)$ and $\rho^* = \rho\sigma^3 = 0.8$.

2. Dipole solute in quadrupolar liquid

We use the reaction field (RF) correction for the cutoff of long-range electrostatic interactions in MC simulations. The interaction energy of a dipolar solute with the quadrupolar solvent is the sum of the interaction energy $u_{0s}^{DQ}(j)$ with the quadrupoles residing within the cutoff sphere and the RF correction terms $u_{0s}^{DQ;RF}$ and $u_{0s}^{DD;self}$

$$u_0 = \sum_j \left[u_{0s}^{DQ}(j) + u_{0s}^{DQ;RF}(j) \right] + u_{0s}^{DD;self}. \quad (\text{B1})$$

where

$$u_{0s}^{DQ}(j) = r_{j0}^{-4} \left[(\hat{\mathbf{r}}_{j0} \cdot \mathbf{Q}_j \cdot \hat{\mathbf{r}}_{j0}) (\mathbf{m}_0 \cdot \hat{\mathbf{r}}_{j0}) - 2 (\hat{\mathbf{r}}_{j0} \cdot \mathbf{Q}_j \cdot \mathbf{m}_0) \right], \quad (\text{B2})$$

and $\mathbf{r}_{j0} = \mathbf{r}_j - \mathbf{r}_0$, $\hat{\mathbf{r}}_{j0} = \mathbf{r}_{j0}/r_{j0}$. In Eq. (B1), $u_{0s}^{DQ;RF}$ is the interaction energy of the solute with the polarization of the dielectric continuum (dielectric constant ϵ') outside the cutoff sphere with the radius R_c

$$u_{0s}^{DQ;RF}(j) = \frac{6(\mathbf{r}_{j0} \cdot \mathbf{Q}_j \cdot \mathbf{m}_0)}{R_c^5} \frac{\epsilon' - 1}{3\epsilon' + 2}. \quad (\text{B3})$$

The term $u_{0s}^{DD;self}$ in Eq. (B1) is the energy of solute self-polarization by the dielectric outside the cutoff:

$$u_{0s}^{DD;self} = -\frac{m_0^2}{R_c^3} \frac{\epsilon' - 1}{2\epsilon' + 1}. \quad (\text{B4})$$

The energy of the j th solvent molecule in the RF geometry is

$$u_{ss}(j) = \sum_{m \neq j} \left[u_{ss}^{QQ}(jm) + u_{ss}^{QQ;RF}(jm) \right] + u_{ss}^{QQ;self}(j) + u_{s0}^{QD}(j). \quad (\text{B5})$$

The quadrupole-quadrupole interaction energy is

$$\begin{aligned} u_{ss}^{QQ}(jm) &= \frac{1}{3r_{mj}^5} \left(35(\hat{\mathbf{r}}_{mj} \cdot \mathbf{Q}_m \cdot \hat{\mathbf{r}}_{mj}) \times \right. \\ &\quad \times (\hat{\mathbf{r}}_{mj} \cdot \mathbf{Q}_m \cdot \hat{\mathbf{r}}_{mj}) - 20(\hat{\mathbf{r}}_{mj} \cdot \mathbf{Q}_j \cdot \mathbf{Q}_m \cdot \hat{\mathbf{r}}_{mj}) \\ &\quad \left. + 2(\mathbf{Q}_j : \mathbf{Q}_m) \right), \end{aligned} \quad (\text{B6})$$

where $\mathbf{r}_{mj} = \mathbf{r}_m - \mathbf{r}_j$, $\hat{\mathbf{r}}_{mj} = \mathbf{r}_{mj}/r_{mj}$, and $\mathbf{Q}_j : \mathbf{Q}_m = \sum_{\nu, \alpha} Q_{j, \nu\alpha} Q_{m, \nu\alpha}$. The interaction energy of the j th

solvent quadrupole with the polarization of the dielectric continuum outside the cavity induced by the m th ($m \neq j$) solvent molecule is

$$u_{ss}^{QQ;RF}(jm) = -\frac{2(\mathbf{Q}_j : \mathbf{Q}_m)}{R_c^5} \frac{\epsilon' - 1}{3\epsilon' + 2}. \quad (\text{B7})$$

The self energy of the j th quadrupole is

$$u_{ss}^{QQ;self}(j) = -\frac{(\mathbf{Q}_j : \mathbf{Q}_j)}{R_c^5} \frac{\epsilon' - 1}{3\epsilon' + 2}. \quad (\text{B8})$$

Finally, $u_{s0}^{QD}(j)$ in Eq. (B5) is equal to $u_{0s}^{DQ}(j)$ from Eq. (B1).

For an axial quadrupole, $\mathbf{Q}_{\nu\alpha, j} = (Q/2)(3\hat{\mathbf{e}}_{\nu, j}\hat{\mathbf{e}}_{\alpha, j} - \delta_{\nu\alpha})$, where $\delta_{\nu\alpha}$ is the Kronecker delta symbol. The interaction potentials are given by

$$\begin{aligned} u_{0s}^{DQ}(j) &= \frac{3m_0Q}{2r_{j0}^4} \left(5(\hat{\mathbf{e}}_j \cdot \hat{\mathbf{r}}_{j0})^2 (\hat{\mathbf{e}}_0 \cdot \hat{\mathbf{r}}_{j0}) \right. \\ &\quad \left. - 2(\hat{\mathbf{e}}_j \cdot \hat{\mathbf{r}}_{j0})(\hat{\mathbf{e}}_0 \cdot \hat{\mathbf{e}}_j) - (\hat{\mathbf{e}}_0 \cdot \hat{\mathbf{r}}_{j0}) \right), \\ u_{ss}^{QQ}(jm) &= \frac{3Q^2}{4r_{mj}^5} \left(1 - 5(\hat{\mathbf{e}}_j \cdot \hat{\mathbf{r}}_{mj})^2 - 5(\hat{\mathbf{e}}_m \cdot \hat{\mathbf{r}}_{mj})^2 \right. \\ &\quad \left. - 20(\hat{\mathbf{e}}_j \cdot \hat{\mathbf{e}}_m)(\hat{\mathbf{e}}_m \cdot \hat{\mathbf{r}}_{mj})(\hat{\mathbf{e}}_j \cdot \hat{\mathbf{r}}_{mj}) \right. \\ &\quad \left. + 35(\hat{\mathbf{e}}_j \cdot \hat{\mathbf{r}}_{mj})^2 (\hat{\mathbf{e}}_m \cdot \hat{\mathbf{r}}_{mj})^2 \right), \\ u_{ss}^{QQ;RF}(jm) &= -\frac{3Q^2}{2R_c^5} \frac{\epsilon' - 1}{3\epsilon' + 2} \left(3(\hat{\mathbf{e}}_j \cdot \hat{\mathbf{e}}_m)^2 - 1 \right), \\ u_{ss}^{QQ;self}(j) &= -\frac{3Q^2}{2R_c^5} \frac{\epsilon' - 1}{3\epsilon' + 2}. \end{aligned} \quad (\text{B9})$$

3. Ionic solute in quadrupolar liquid

For ion solvation simulations we use the RF approximation for the solvent-solvent interactions [Eq. (B9)] and the Ewald sum (ES) approximation for the solute-solvent interactions. The solute energy is

$$u_{0s} = \sum_{j=1}^N u_{0s}^{CQ}(j) + u_{0s}^{CC;self}, \quad (\text{B10})$$

where $u_{0s}^{CC;self}$ is the self energy term and $u_{s0}^{CQ}(j)$ is the interaction energy of the solute with the j th solvent molecule. The self energy is the interaction energy of the solute charge with its images in replicas of the simulation box

$$u_{0s}^{CC;self} = -\frac{q_0^2}{L} \left(\frac{\xi_{EW}}{2} + \frac{\pi}{6} \left(\frac{\sigma_0}{L} \right)^2 - \frac{\pi^2}{180} \left(\frac{\sigma_0}{L} \right)^5 \right), \quad (\text{B11})$$

where the finite-size correction $\xi_{EW} = 1.41865$ is according to Hunenberger and McCammon,⁸² σ_0 is the hard-sphere solute diameter, and L is the side length of the cubic simulation box.

The interaction energy of the solute with the j th solvent molecules is (q_0 is the solute charge)

$$u_{0s}^{CQ}(j) = \frac{q_0}{3} (\hat{\mathbf{r}}_{j0} \cdot \mathbf{Q}_j \cdot \hat{\mathbf{r}}_{j0}) \left[f_2(r_{j0}) + \frac{3}{r_{j0}^3} f_1(r_{j0}) \right] - \frac{4q_0\pi}{3L^3} \sum_{|\mathbf{k}| \neq 0} \exp(-k^2/4\kappa^2) \cos(\mathbf{k} \cdot \mathbf{r}_{j0}) (\hat{\mathbf{k}} \cdot \mathbf{Q}_j \cdot \hat{\mathbf{k}}), \quad (\text{B12})$$

where

$$f_1(x) = \text{erfc}(\kappa x) + \frac{2\kappa x \exp(-x^2 \kappa^2)}{\sqrt{\pi}}, \quad (\text{B13})$$

$$f_2(x) = \frac{4\kappa^3 \exp(-x^2 \kappa^2)}{\sqrt{\pi}}.$$

and $\text{erfc}(x) = 1 - \text{erf}(x)$, $\text{erf}(x)$ is the error function.⁶⁰ The solute-solvent interaction potential consists of two parts. The first is taken in the real \mathbf{r} -space, while the second is taken in the inverted \mathbf{k} -space. The convergence parameter κ defines the number of replicas of the simulation cell to be taken in the real space. Additionally, it defines the number of \mathbf{k} -vectors taken in the inverted space sum. When this parameter is sufficiently large the calculation the real space sum is restricted to the original simulation box.⁸¹

Finally, the interaction energy of the j th molecule of the solvent is

$$u_s(j) = u_{ss}^{QQ}(j) + u_{ss}^{QQ;RF}(j) + u_{ss}^{QQ;\text{self}}(j) + u_{s0}^{QC}(j), \quad (\text{B14})$$

where the first three terms are given by Eq. (B9), $u_{s0}^{QC}(j) = u_{0s}^{CQ}(j)$ [Eq. (B12)], and the last term is given by Eq. (B12).

APPENDIX C: DETAILS OF MD SIMULATIONS OF BENZENE

The MD simulations were carried out with the force field of 12-site benzene by Danten *et al.*⁶¹ (Table X). The site-site interaction is given by the sum of the Lennard-Jones (LJ) and Coulomb interaction potentials:

$$E^{ab} = 4\epsilon^{ab} \left[\left(\frac{\sigma^{ab}}{r^{ab}} \right)^{12} - \left(\frac{\sigma^{ab}}{r^{ab}} \right)^6 \right] + \frac{q^a q^b}{r^{ab}}, \quad (\text{C1})$$

where the LJ parameters are taken according to the Lorentz-Bertholet rules: $\epsilon^{ab} = \sqrt{\epsilon^a \epsilon^b}$ and $\sigma^{ab} = (\sigma^a + \sigma^b)/2$. All simulations were done with the DL_POLY molecular dynamics package.⁸³ We run MD simulations in the temperature range from 298 K to 342 K with a 14 K step. The timestep in each simulation is 5 fs. All MD simulation are 10 ns long.

We used the Nosé-Hoover⁸⁴ thermostat with the relaxation parameter 0.5 fs. The proper choice of the simulation timestep and the relaxation parameter ensures

low drift in the total energy of about 0.3%. Cut-off distance of 12 Å is used in calculations of LJ interactions. Ewald summation parameters used in calculations are: (1) the convergence parameter $\kappa = 0.265 \text{ \AA}^{-1}$; (2) the maximum wavelength $k_{x,y,z}^{\text{max}} = 7 \text{ \AA}^{-1}$. The simulation box is constructed to include 125 benzene molecules in a cube with the side length $L = 26.46 \text{ \AA}$ at $T = 298 \text{ K}$ to reproduce the experimental mass density of benzene,⁸⁵ $\rho_M = 0.874 \text{ g/cm}^3$. The side length is adjusted at each temperature to give the correct experimental value for the isobaric temperature expansion coefficient,⁸⁵ $\alpha_p = 1.14 \times 10^{-3} \text{ K}^{-1}$.

TABLE X: Force field of benzene used in the MD simulation.

Interaction site ^a	$\sigma^a/\text{\AA}$	$\epsilon^a \times 10^2/(\text{kcal/mol})$	q^a/e
C	3.473	83.1	-0.153
H	2.945	12.5	0.153

$${}^a r_{\text{CC}} = 1.393 \text{ \AA}, r_{\text{CH}} = 1.027 \text{ \AA}.$$

APPENDIX D: CALCULATION ALGORITHM FOR $\tilde{\phi}_{\alpha\beta}(\mathbf{k})$

The gradient of the solute electric field $\phi_{\alpha\beta}(\mathbf{r})$ is calculated on the 256^3 grid in \mathbf{r} -space (Fig. 13) as defined by Eq. (15). In order to speed up the calculations, we split the calculation of the Fourier transform $\tilde{\phi}_{\alpha\beta}(\mathbf{k})$ into two regions. In region Ω_1 , the Fourier transform is calculated numerically with a fast Fourier transform (FFT) algorithm.⁸⁶ In region Ω_2 , the multipole expansion of the set of solute charges is used, and the Fourier transform is calculated analytically. The total $\tilde{\phi}_{\alpha\beta}(\mathbf{k})$ is the sum of Fourier transforms from each region

$$\tilde{\phi}_{\alpha\beta}(\mathbf{k}) = \tilde{\phi}_{\alpha\beta;\Omega_1}(\mathbf{k}) + \tilde{\phi}_{\alpha\beta;\Omega_2}(\mathbf{k}). \quad (\text{D1})$$

The analytical part of Fourier transform for an arbitrary distribution of solute atomic charges q_0^a with coordinates \mathbf{r}_0^a , $r_0^a < R_1$ is given by

$$\tilde{\phi}_{\alpha\beta;\Omega_2}(\mathbf{k}) = -4\pi \sum_{a=1}^M q_0^a \sum_{n=2}^{\infty} (-i)^n \left(\frac{r_0^a}{R_1} \right)^{n-2} \frac{j_{n-1}(kR_1)}{kR_1} \times (\hat{r}_{0\alpha}^a \hat{r}_{0\beta}^a P''_{n-2}(x^a) - \delta_{\alpha\beta} P'_{n-1}(x^a) - (\hat{k}_\alpha \hat{r}_{0\beta}^a + \hat{r}_{0\alpha}^a \hat{k}_\beta) P''_{n-1}(x^a) + \hat{k}_\alpha \hat{k}_\beta P'_n(x^a)). \quad (\text{D2})$$

Here, R_1 is the radius of the sphere enclosing volume Ω_1 , $j_n(x)$ is the spherical Bessel function of the order n ,⁶⁰ $P_n(x)$ is the Legendre polynomial of order n , $P'_n(x) = dP_n(x)/dx$ and $P''_n(x) = d^2P_n(x)/dx^2$, $x^a = \hat{\mathbf{k}} \cdot \hat{\mathbf{r}}_0^a$.

The volume of integration for the numerical FFT is a cubic box of side length

$$L_{\text{grid}} = f \times R_{\text{max}} \quad (\text{D3})$$

obtained as a multiple of the maximum extension of the solvent inaccessible cavity, given by the radius R_{max} . The

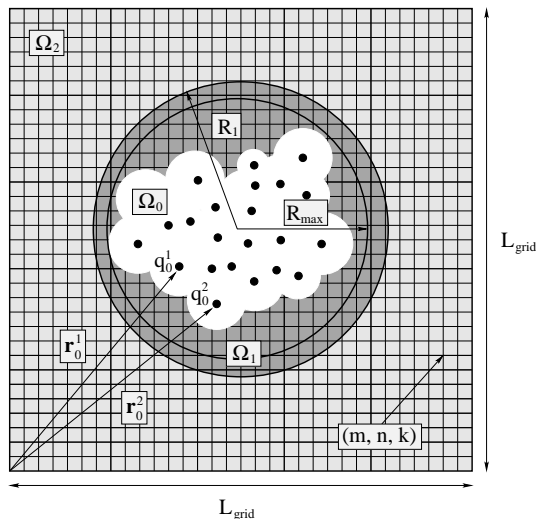


FIG. 13: The schematic representation of the calculation geometry. Ω_0 is the solvent inaccessible cavity. Ω_1 (space between the sphere of radius R_1 and Ω_0) is the region of the numerical Fourier transform of $\phi_{\alpha\beta}(\mathbf{r})$ [Eq. (15)]. Ω_2 is the region where Fourier transform of $\phi_{\alpha\beta}(\mathbf{r})$ is taken analytically [Eq. (D2)]. R_{\max} is the radius of the sphere defining solute maximum extension and $R_1 = R_{\max} + \sigma/2$. The length $L_{\text{grid}} = 9 \times R_{\max}$ is the size of the \mathbf{r} -space grid of dimension $256 \times 256 \times 256$; (m, n, k) is the position of a point on the grid.

radius of the sphere of the solute maximum extension is defined as

$$R_{\max} = \max \{ |\mathbf{r}_0^a - \mathbf{r}_{\text{gc}}| + \sigma_0^a/2 \}, \quad (\text{D4})$$

where i runs over M solute atoms. The sphere is centered at the geometric center of the solute molecule, $\mathbf{r}_{\text{gc}} = (1/M) \sum_a \mathbf{r}_0^a$ and σ_0^a is the diameter of atom a of the solute. The radius of the spherical region Ω_1 is the obtained by adding the solvent radius $\sigma/2$ to R_{\max} : $R_1 = R_{\max} + \sigma/2$ (Fig. 13). The multiplication factor $f = 9$ in Eq. (D3) is chosen as a trade-off between minimizing FFT errors from artificial periodicity of the lattice sum and the need for a sufficiently small increment in the \mathbf{k} -space for the \mathbf{k} -integration.

Charges of complex **1** in the non-polar (initial) and charge-transfer (final) states are calculated with **Gaussian**'03 (UHF/6-31G(3p)).⁸⁷ Partial atomic charges are obtained by fitting to the electrostatic potential given by the exact wavefunction in the CHELPG scheme.⁸⁸ Charges are calculated separately for the isolated donor, donor cation, acceptor, acceptor anion, and the neutral bridge. The charges of the two hydrogens that substitute the rest of the clamp in the model compounds are incorporated in the connected carbon atoms.⁷⁰

- ¹ D. V. Matyushov and R. Schmid, *J. Chem. Phys.* **103**, 2034 (1995).
- ² L. Reynolds, J. A. Gardecki, S. J. V. Frankland, and M. Maroncelli, *J. Phys. Chem.* **100**, 10337 (1996).
- ³ B. M. Ladanyi and M. Maroncelli, *J. Chem. Phys.* **109**, 3204 (1998).
- ⁴ D. S. Larsen, K. Ohta, and G. R. Fleming, *J. Chem. Phys.* **111**, 8970 (1999).
- ⁵ D. V. Matyushov and G. A. Voth, *J. Chem. Phys.* **111**, 3630 (1999).
- ⁶ F. O. Raineri and H. L. Friedman, *Adv. Chem. Phys.* **107**, 81 (1999).
- ⁷ M. D. Stephens, J. G. Saven, and J. L. Skinner, *J. Chem. Phys.* **106**, 2129 (1997).
- ⁸ M. Berg, *J. Phys. Chem. A* **102**, 17 (1998).
- ⁹ B. Bagchi and R. Biswas, *Adv. Chem. Phys.* **109**, 207 (1999).
- ¹⁰ T. Yamaguchi, Y. Kinura, and M. Nakahara, *J. Phys. Chem. B* **106**, 9126 (2002).
- ¹¹ S. A. Egorov, R. A. Denny, and D. R. Reichman, *J. Chem. Phys.* **116**, 5080 (2002).
- ¹² The term non-polar solvation is often associated with all situations when either the solute or the solvent do not possess both charge and dipole moment. We limit ourselves here with a more narrow case of an ionic or dipolar solute in a non-dipolar solvent.
- ¹³ H. Reiss, H. L. Frisch, and J. L. Lebowitz, *J. Chem. Phys.* **31**, 369 (1959).
- ¹⁴ A. Stamatopoulou and D. Ben-Amotz, *J. Chem. Phys.* **106**, 1181 (1997).
- ¹⁵ D. V. Matyushov and B. M. Ladanyi, *J. Chem. Phys.* **107**, 5815 (1997).
- ¹⁶ D. Ben-Amotz and I. P. Omelyan, *J. Chem. Phys.* **115**, 9401 (2001).
- ¹⁷ M. Heying and D. S. Corti, *J. Phys. Chem. B* **108**, 19756 (2004).
- ¹⁸ D. V. Matyushov, R. Schmid, and B. M. Ladanyi, *J. Phys. Chem. B* **101**, 1035 (1997).
- ¹⁹ J. T. Fourkas, A. Benigno, and M. Berg, *J. Non-Cryst. Sol.* **172-174**, 234 (1994).
- ²⁰ V. Tran and B. J. Schwartz, *J. Phys. Chem. B* **103**, 5570 (1999).
- ²¹ J. Jeon and H. J. Kim, *J. Sol. Chem.* **30**, 849 (2001).
- ²² J. Jeon and H. J. Kim, *J. Chem. Phys.* **119**, 8606 (2003).
- ²³ J. Jeon and H. J. Kim, *J. Chem. Phys.* **119**, 8626 (2003).
- ²⁴ S. Nugent and B. M. Ladanyi, *J. Chem. Phys.* **120**, 874 (2004).
- ²⁵ P. F. Barbara and W. Jarzeba, *Adv. Photochem.* **15**, 1 (1990).
- ²⁶ B. Bagchi and A. Chandra, *Adv. Chem. Phys.* **80**, 1 (1991).
- ²⁷ G. van der Zwan and J. T. Hynes, *J. Phys. Chem.* **89**, 4181 (1985).
- ²⁸ L. E. Fried and S. Mukamel, *J. Chem. Phys.* **93**, 932 (1990).
- ²⁹ M. Maroncelli, *J. Mol. Liq.* **57**, 1 (1993).
- ³⁰ M. L. Horng, J. A. Gardecki, A. Papazyan, and M. Maroncelli, *J. Phys. Chem.* **99**, 17311 (1995).
- ³¹ C.-P. Hsu, X. Song, and R. A. Marcus, *J. Phys. Chem. B* **101**, 2546 (1997).
- ³² J. Morais and M. B. Zimmt, *J. Phys. Chem.* **99**, 8863

- (1995).
- ³³ J. F. Kauffman, *J. Phys. Chem. A* **105**, 3433 (2001).
- ³⁴ B. M. Britt, J. L. McHale, and D. M. Friedrich, *J. Phys. Chem.* **99**, 6347 (1995).
- ³⁵ K. Kulinowski, I. R. Gould, and A. B. Myers, *J. Phys. Chem.* **99**, 9017 (1995).
- ³⁶ M. B. Zimmt and D. H. Waldeck, *J. Phys. Chem. A* **107**, 3580 (2003).
- ³⁷ D. V. Matyushov, *J. Chem. Phys.* **120**, 7532 (2004).
- ³⁸ A. Milischuk, D. V. Matyushov, and M. D. Newton, *Chem. Phys.* p. to be submitted (2005).
- ³⁹ D. Chandler, *Phys. Rev. E* **48**, 2898 (1993).
- ⁴⁰ L. Onsager, *J. Am. Chem. Soc.* **58**, 1486 (1936).
- ⁴¹ C. J. F. Böttcher, *Theory of Electric Polarization*, vol. 1 (Elsevier, 1973).
- ⁴² R. M. Ernst, L. Wu, C.-H. Liu, S. R. Nagel, and M. E. Neubert, *Phys. Rev. B* **45**, 667 (1992).
- ⁴³ B. Widom, *Science* **157**, 357 (1967).
- ⁴⁴ W. M. Gelbart and B. A. Baron, *J. Chem. Phys.* **66**, 207 (1977).
- ⁴⁵ A. Milischuk and D. V. Matyushov, *J. Phys. Chem. A* **106**, 2146 (2002).
- ⁴⁶ X. Song and D. Chandler, *J. Chem. Phys.* **108**, 2594 (1998).
- ⁴⁷ D. V. Matyushov, *J. Chem. Phys.* **120**, 1375 (2004).
- ⁴⁸ C. G. Gray and K. E. Gubbins, *Theory of Molecular Liquids* (Clarendon Press, Oxford, 1984).
- ⁴⁹ P. Madden and D. Kivelson, *Adv. Chem. Phys.* **56**, 467 (1984).
- ⁵⁰ D. V. Matyushov, *Chem. Phys.* **174**, 199 (1993).
- ⁵¹ T. Fonseca and B. M. Ladanyi, *J. Chem. Phys.* **11**, 8148 (1990).
- ⁵² F. Raineri and H. Friedman, *J. Chem. Phys.* **98**, 8910 (1993).
- ⁵³ P. A. Bopp, A. A. Kornyshev, and G. Sutmann, *Phys. Rev. Lett.* **76**, 1280 (1996).
- ⁵⁴ B.-C. Perng, M. D. Newton, F. O. Raineri, and H. L. Friedman, *J. Chem. Phys.* **104**, 7153 (1996).
- ⁵⁵ M. S. Skaf, *J. Chem. Phys.* **107**, 7996 (1997).
- ⁵⁶ P. A. Bopp, A. A. Kornyshev, and G. Sutmann, *J. Chem. Phys.* **109**, 1939 (1998).
- ⁵⁷ I. P. Omelyan, *Mol. Phys.* **407**, 407 (1999).
- ⁵⁸ B.-C. Perng and B. M. Ladanyi, *J. Chem. Phys.* **110**, 6389 (1999).
- ⁵⁹ G. Stell, G. N. Patey, and J. S. Høye, *Adv. Chem. Phys.* **18**, 183 (1981).
- ⁶⁰ M. Abramowitz and I. A. Stegun, eds., *Handbook of Mathematical Functions* (Dover, New York, 1972).
- ⁶¹ Y. Danten, B. Guillot, and Y. Guissani, *J. Chem. Phys.* **96**, 3782 (1992).
- ⁶² L. L. Lee and D. Levesque, *Mol. Phys.* **26**, 1351 (1973).
- ⁶³ R. Schmid and D. V. Matyushov, *J. Phys. Chem.* **99**, 2393 (1995).
- ⁶⁴ D. V. Matyushov and R. Schmid, *J. Chem. Phys.* **104**, 8627 (1996).
- ⁶⁵ I. Read, R. Kaplan, M. B. Zimmt, and D. H. Waldeck, *J. Am. Chem. Soc.* **121**, 10976 (1999).
- ⁶⁶ I. Read, A. Napper, M. B. Zimmt, and D. H. Waldeck, *J. Phys. Chem. A* **104**, 9385 (2000).
- ⁶⁷ K. Kumar, Z. Lin, D. H. Waldeck, and M. B. Zimmt, *J. Am. Chem. Soc.* **118**, 243 (1996).
- ⁶⁸ W. L. Jorgensen, D. S. Maxwell, and J. Tirado-Rives, *J. Am. Chem. Soc.* **118**, 11225 (1996).
- ⁶⁹ P. Vath, M. B. Zimmt, D. V. Matyushov, and G. A. Voth, *J. Phys. Chem. B* **103**, 9130 (1999).
- ⁷⁰ A. Troisi, M. A. Ratner, and M. B. Zimmt, *J. Am. Chem. Soc.* **126**, 2215 (2004).
- ⁷¹ I. Renge, *Chem. Phys.* **167**, 173 (1992).
- ⁷² W. Rocchia, E. Alexov, and B. Honig, *J. Phys. Chem. B* **105**, 6507 (2001).
- ⁷³ D. V. Matyushov and B. M. Ladanyi, *J. Chem. Phys.* **110**, 994 (1999).
- ⁷⁴ R. Ramirez, R. Gebauer, M. Mareschal, and D. Borgis, *Phys. Rev. E* **66**, 031206 (2002).
- ⁷⁵ R. Ramirez and D. Borgis, *J. Phys. Chem. B* **109**, 6754 (2005).
- ⁷⁶ S. Dorairaj and H. J. Kim, *J. Phys. Chem. A* **106**, 2322 (2002).
- ⁷⁷ T. Yamaguchi and F. Hirata, *J. Chem. Phys.* **117**, 2216 (2002).
- ⁷⁸ D. V. Matyushov and R. Schmid, *Mol. Phys.* **84**, 533 (1995).
- ⁷⁹ D. V. Matyushov, *Mol. Phys.* **79**, 795 (1993).
- ⁸⁰ M. Khajepour and J. F. Kauffman, *J. Phys. Chem. A* **104**, 9512 (2000).
- ⁸¹ M. P. Allen and D. J. Tildesley, *Computer Simulation of Liquids* (Clarendon Press, Oxford, 1996).
- ⁸² P. H. Hunenberger and J. A. McCammon, *J. Chem. Phys.* **110**, 1856 (1999).
- ⁸³ W. Smith and T. R. Forester, *J. Molec. Graphics* **14**, 136 (1996).
- ⁸⁴ W. G. Hoover, *Phys. Rev. A* **31**, 1695 (1985).
- ⁸⁵ *CRC Handbook Chemistry and Physics* (CRC Press, 2005), 85th ed.
- ⁸⁶ W. H. Press, S. A. Teukolsky, W. T. Vetterling, and B. P. Flannery, *Numerical recipes in Fortran 77: The art of scientific computing* (Cambridge University Press, 1996).
- ⁸⁷ M. J. Frisch, G. W. Trucks, H. B. Schlegel, G. E. Scuseria, M. A. Robb, J. R. Cheeseman, J. J. A. Montgomery, T. Vreven, K. N. Kudin, J. C. Burant, et al., Gaussian, Inc., Pittsburgh PA (2003).
- ⁸⁸ C. M. Breneman and K. B. Wiberg, *J. Comp. Chem.* **11**, 361 (1990).